Journal of Ultrafine Grained and Nanostructured Materials
https://jufgnsm.ut.ac.ir
Vol. 58, No.2, June 2025, pp. 161-196
Print ISSN: 2423-6845 Online ISSN: 2423-6837
DOI: 10.22059/jufgnsm.2025.02.04

Ultrasonic surface severe plastic deformation of selective laser melted metal parts-A review

R. Taghiabadi

Department of Materials Science and Metallurgy, Imam Khomeini International University, Qazvin, IRAN, Tel.: +98-28 33901143

Recieved: 26 July 2025; Accepted: 17 August 2025

*Corresponding author, E-mail: taghiabadi@ikiu.ac.ir

ABSTRACT

Selective laser melting (SLM) is cobsidered as a promising method in additive manufacturing (AM), especially for producing complex metallic parts. The SLM market is witnessing substantial growth, fueled by rising demand for cutting-edge manufacturing solutions in multiple sectors, and is expected to hit $5.8 billion by 2032. Nonetheless, SLMed parts suffer from problems such as process-related defects, tensile residual stress (TRS), and improper surface finish, which may restrict their industrial application. On this basis, this review studies the latest advancements in the field of post-processing of SLMed components utilizing ultrasonic-based surface severe plastic deformation (US-SSPD) methods. It is noteworthy that ultrasonic technology is progressively acknowledged as an eco-friendly metal processing technique, providing benefits like enhanced energy efficiency, lower chemical consumption, and greater sustainability. The results revealed that regardless of the material being investigated, applying US-SSPD is likely to modify the surface microstructure, promote the formation of ultrafine grains/nanostructures, decrease the porosity content, modify the surface roughness, and convert the undesirable TRS to the compressive residual stresses (CRS) causing notable improvement in surface mechanical properties, fatigue strength, corrosion resistance, and tribological characteristics.

Keywords: *Selective laser melting (SLM), Laser powder bed fusion (LPBF), Post-processing, Ultrasonic, Surface severe plastic deformation (SSPD), Additive manufacturing (AM).*

1. Introduction

The AM technique entails the sequential addition of layers of materials to create complex 3D parts based on a specified computer-aided design (CAD) model. It is very appealing for complex designs and economical for limited runs, finding extensive use in various industrial sectors such as automotive, aerospace, and biomedical applications [1-4]. AM has advantages over traditional manufacturing techniques encompassing the removal of numerous production stages, freedom in design, customizable complexity with near-net shape components, the ability to bypass tooling, enhanced personalization, the capacity to create parts ranging from macro to micro dimensions, efficient material consumption with reduced waste, ease in producing updated versions of products, one-step creation of hollow or lattice structures, and on-demand sourcing of specific components at relatively lower costs [5-8].

Depending on the processes and materials used, AM can be divided into various subcategories, with SLM or LPBF being the most notable. The SLM offers significant benefits compared to traditional manufacturing methods, such as minimal restrictions in part geometry, excellent processing accuracy, and near-net-shape production.

Consequently, a variety of metallic materials, including different steel grades, superalloys, and non-ferrous alloys based on Cu, Ti, Ta, W, Al, Mg, have been SLMed to study their potential uses in turbo-engines, biomedical implants, and molds featuring internal conformal cooling channels [1,9-12].

Based on the literature, nearly all SLMed components cannot directly be used in service. Further thermal and/or mechanical treatments are required to overcome their common issues such as high surface roughness, coarse (columnar) grained structure, surface/subsurface porosities, poor ductility, dimensional mismatch, high TRS, and weak corrosion/wear behavior [1,10,12]. Thus, various techniques have been developed for the post-processing of SLMed components; among which, SSPD methods, particularly those based on ultrasonic treatment, have allured researchers and scientists [13-15]. This is because, in spite of their proven capabilities, the common post-processing techniques such as heat treatment and hot isostatic pressing (HIP) usually impair the hardness/strength of the SLMed parts [16-18]. For instance, the fine structure/grains of the rapidly-solidified SLMed parts coarsened after heat treatment at higher temperatures. . In additionit does not have a positive effect on the surface quality of the SLMed parts and cannot reduce their porosity content [19]. Reports have also shown that despite its reducing effect on the porosity content, applying HIP increases surface roughness of SLMed parts [19].

The failure of engineering parts frequently begins at their surface, and improving the surface properties is likely to enhance their performance/lifespan. Therefore, US-SSPD-based post-processing methods are considered as alternative post-processing methods for the performance improvement of SLMed components, due to the localized plastic (surface) deformation, surface microstructural modification/creation of ultrafine/nano-sized grains, alleviation of surface TRSs, and simultaneous enhancement of the strength and ductility, [20].

On this basis, this research aims to evaluate for the first time the most recent studies performed in the area of surface characteristics enhancement of SLMed components using ultrasonic energy. Given the growing popularity of the SLM technique, the ultimate goal is to prepare a comprehensive review paper covering the latest research on ultrasonic post-processing of SLMed parts. Before reviewing the relevant literature, an attempt is made to provide a preliminary explanation of the SLM process and its disadvantages and defects. Then, the most important SSPD processes are examined with an emphasis on processes based on ultrasonic waves.

2. Selective laser melting (SLM)

2.1. Background on SLM

SLM is an AM process established by M. Fockele and D. Schwarze from F&S Stereolithographietechnik GmbH, alongside W. Meiners, K. Wissenbach, and G. Andres from Fraunhofer ILT, aimed at the production of metallic parts from metal powders. The SLM process employs a high-intensity laser as the energy source to melt and fuse specific areas of powder, layer by layer, based on CAD data. The patent for this technology was initially submitted in 1997 to the German Patent and Trade Mark Office and released in 1998. In 2001, a patent was additionally filed by Das and Beaman due to their groundbreaking research in direct selective laser sintering [10]. As lots of contributions show, the SLM method is now rather well developed to make a large number of alloys with static mechanical properties that are comparable to those of wrought ones.

2.2. Description of the procedure

As mentioned earlier, SLM is among the most commonly utilized 3D printing (AM) methods for the production of metallic parts, where metal powders serve as the raw materials. The principles of melting and scanning in SLM are schematically depicted in Fig. 1a and 1b, respectively, where a high-energy laser beam selectively melts metal powders according to CAD data and locally fuses them with the underlying layer. After the laser scanning finishes, the powder bed is slightly lowered, and the subsequent layer of powder is applied and illuminated locally with the laser. This periodic method enables the construction of components one layer at a time (Fig. 2) [21-24].

Throughout the SLM procedure, the process chamber is frequently purged with N_2 or Ar to minimize oxidation. To compromise between attaining fine resolution and facilitating good powder flowability, the thickness of the layer typically varies between 20 and 100 μm. Powders with larger particle sizes lead to diminished resolution and build tolerance, while smaller powders tend to agglomerate together easily because of van der Waals forces, leading to inadequate powder flowability and subsequent poor powder deposition. The laser beam in the focal plane usually measures between 50 and 80 μm and the scanning velocity can reach significant levels (up to 15 m/s). The cooling rate throughout the process can also attain levels as high as 10^4-10^6 K/s. These high cooling rates form the basis for the refinement of microstructures in crystalline materials or the formation of glasses in glass-forming alloys [21].

2.3. Parameters affecting the SLM production

The factors influencing the performance of SLM products primarily consist of laser-associated

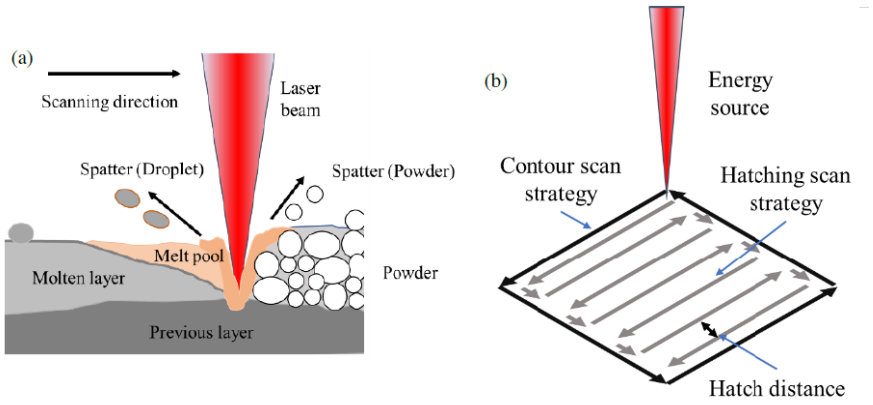

Fig. 1- Schematic diagrams showing (a) melting and (b) scanning techniques in the SLM [22].

Fig. 2- Example of parts produced by SLM technique fastened to the build plate with supports [22].

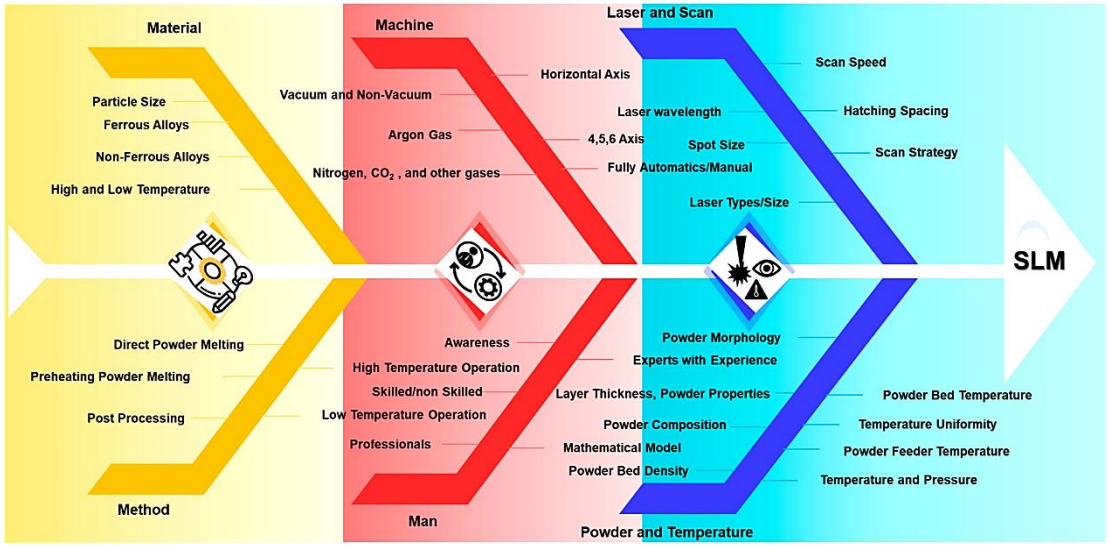

Fig. 3- Fishbone diagram depicting the causal elements and their impacts on the quality of components produced via SLM [25].

parameters, including laser scanning power, scanning velocity, fill distance, scanning strategy, and laser spot size, along with construction-related parameters like layer thickness, build orientation, and molding [9]. Fig. 3 illustrates different elements influencing the quality of SLMed products. These elements comprise [25]:

- Powder metal characteristics, including its average size, morphology, composition, and melting point range;
- The machine parameters such as inert gas atmosphere, chamber temperature , configuration of axes, and initial duration of laser heating;
- Parameters related to laser and scanning, including scan speed, hatching duration, spacing, spot size, and layer thickness;
- Pre- and post-processing techniques encompass preheating and methods for relieving residual stress;
- The operator's expertise and background;
- The relationship between powder and temperature. Mismatching a low-melting powder with a high operational temperature may result in the incorrect execution of intended commands.

Thus, understanding and effectively managing these factors is crucial for attaining the intended results in the SLM process. Currently, techniques like the Taguchi method, response surface methodology (RSM), and trial-and-error assist in optimizing process parameters and enhancing the understanding of the elements affecting the manufacturing of components with required characteristics [25].

2.4. Negative aspects and defects in SLM

In spite of its advantages, the SLM involves complex physics, including laser energy absorption/transmission, rapid melting and solidification, high thermal gradient, varying G/R ratio, unsteady Marangoni flow in a molten pool, uneven contraction and expansion, and material evaporation. Therefore, to achieve high-quality parts, exact control of process parameters is of great importance [26,27]. Otherwise, various defects may be introduced into the SLMed parts, shortening their service life.

The most noticeable and apparent drawback in SLMed parts is the poor surface finish resulting from the staircase effect caused by layer-by-layer production, the balling effect, and the presence of open pores/areas with incomplete melting [19]. Improper surface roughness not only impairs the dimensional accuracy of the SLMed components but also adversely affects their mechanical (fatigue), corrosion, and tribological characteristics [1,28].

High porosity content and micro-segregation are other critical issues in SLMed components. The porosities are generally caused by gas entrapment within the metal from vapor backlash in the course of the process and/or voids that arise between unmelted particles. While acting as stress concentrators, micropores can also greatly reduce the critical stress needed for microcrack initiation, thereby considerably undermining the hardness, tensile, and fatigue properties, corrosion behavior, and tribological properties of metals [19,29]. Micro-segregation is an inevitable phenomenon during the SLM process. However, due to the high solidification cooling rate applied [30], its range was reported to be low when compared to the conventionally-cast alloys, leading to a considerably uniform microstructure [31,32]. According to the literature [32], the effects of micro-segregation on the properties of SLMed parts are controversial [32]. While some reports indicate its positive impacts [33,34], many other reports have emphesized its negative effect on the mechanical properties, fatigue strength, corrosion resistance, and hot tearing resistance of SLMed parts [32]. Accordingly, efforts have been made to minimize segregation by optimizing the process parameters such as increasing the laser beam scanning speed [31], using specific production techniques (e.g., pulsed lasers [32]), and/or using post-processing techniques such as heat treatment [29,35,36], HIP [29,37], and electropulsing treatment [38]. SLM processing can also readily create internal microcracks resulting from stresses caused by rapid powder melting as well as high temperature gradients [27]. These microcracks greatly diminish the dimensional accuracy and mechanical characteristics of SLMed samples [26].

Eventually, due to the high thermal gradients (on the order of 5×10^4 K/cm) [19], the SLMed components are prone to developSRSs. If not addressed, these stresses can lead to distortion, cracking, failure, and reduced geometrical accuracy of the SLMed components, decreasing their mechanical/wear/corrosion performance [19]. The RS distribution typically features significant tensile stress in both the upper and lower sections of the SLMed sample, with notable compressive stress in the larger central region [26].

Nonetheless, it has been acknowledged that even when the optimal process parameters are chosen, defects may still form due to other factors, including an out-of-calibration system and fluctuation in the flow of purging gas in the course of the process. Consequently, process optimization is unable to fully address the three main problems with the SLM process, namely high porosity, low surface quality, and undesirable (tensile) residual stresses. Therefore, post-processing techniques must be utilized to enhance the actual effectiveness of SLMed components by modifying their surface integrity and their densification and changing

their surface TRSs into the desirable compressive stresses [26,27].

3. Post-processing of SLMed metallic parts

From the preceding sections it appears that the SLM-processed metal parts typically exhibit a comparatively rough and uneven surface [1,2,37], surface/subsurface porosity [39-41], micro-segregation [30], significant TRSs in the near-surface regions [42], columnar grains characterized by anisotropy [42,43], and the dimensional/orientation variations within the grain structure. The combined impact of these adverse factors undermines the surface characteristics of SLMed metal parts and restricts their extensive use despite their significant potential [44]. Nonetheless, post-processing techniques are highly effective in enhancing the characteristics of SLMed metals. Common post-processing techniques include heat treatment, mechanical or deformation-based surface finishing, HIP, shot peening (SP), blasting, polishing) [19,45], chemical polishing, chemically-assisted magnetic abrasive finishing process (CMAF) [46], combined chemical-abrasive flow polishing [47], laser shock peening (LSP) [46], and laser polishing/laser texturing, ultrasonic nanocrystal surface modification (UNSM), etc. [19,48-50].

4. Surface severe plastic deformation (SSPD) processes

SSPD techniques are a category of surface treatment methods employed to improve the materials' mechanical properties by creating a plastically deformed surface layer. In SSPD, functional microstructures are developed from the surface towards the the sample's interior rather than forming an even plastically-deformed microstructure. Achieving this structural feature is especially important when the surface of the component is exposed to surface-destructive phenomena such as wear, corrosion, and fatigue in applications such as biomedical, automotive, and aerospace.

4.1. Overview of SSPD procedures

As a successful technique for producing ultrafine grain (UFG) materials and nanocrystalline microstructures comprising significant crystal lattice defects, such as vacancies, dislocations, and grain boundaries, SPD is attracting a lot of attention and is finding a wide range of applications [51-53]. These superior properties have also attracted the attention of many researchers, where the volume of publications concerning SPD has steadily increased since 2000, with more than 1000 papers being published annually on the topic of SPD (Fig. 4) [51].

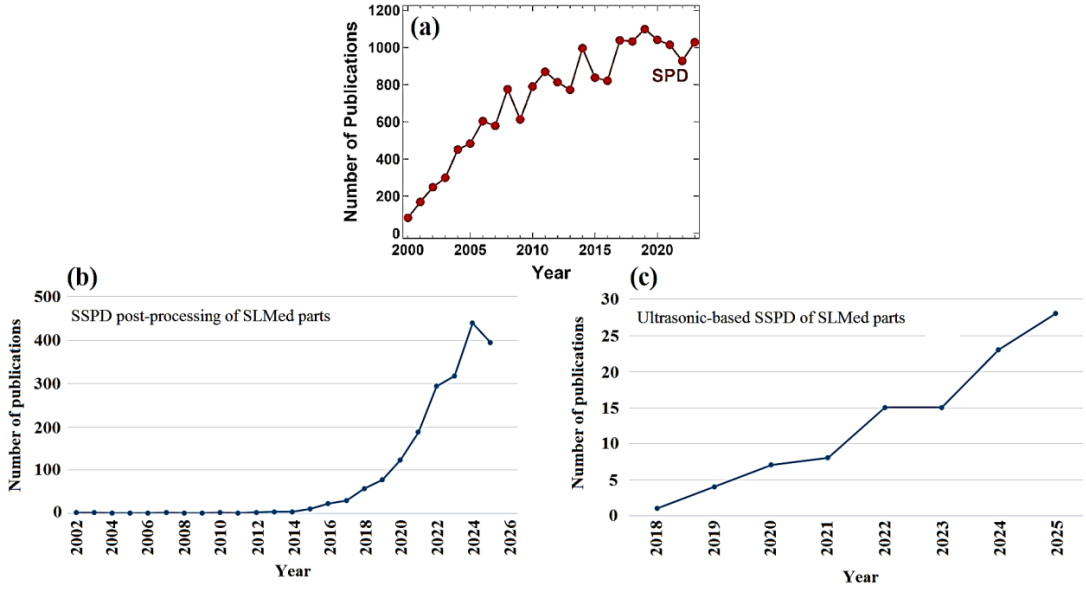

Fig. 4- Trend of annual publications in the field of (a) SPD processes [51], (b) SSPD post-processing of SLMed parts, and (c) US-SSPD post-processing of SLMed parts.

The SPD techniques can be classified into three distinct categories, namely, bulk processing, surface processing, and powder processing. Although the surface is also affected, the goal in the former scenario is to change the bulk microstructure of materials. In contrast, the bulk of the sample remains largely unaltered in SSPD, with only the surface and subsurface layers changing [54]. SSPD processes provide notable technological benefits for commercial applications when surface properties like corrosion resistance, wear resistance, and biocompatibility are essential [51,52]. Over the years, numerous techniques have been developed to create SSPD, such as sand blasting, air blast shot peening (ABSP), surface mechanical rolling treatment (SMRT), occasionally called surface mechanical grinding treatment (SMGT), laser shock peening (LSP), fast multiple rotation rolling (FMRR), ball burnishing (BB), flap peening, micro-shot peening, acoustic/hydrodynamic cavitation peening, and friction-based methods (friction stirring, friction hardening) [51-53, 55]. A statistical analysis of the number of articles published over the past years (Fig. 4b) also indicates a significant interest among researchers in this topic.

4.2. SSPD processes utilizing ultrasonic technology

In ultrasonic surface treatment processes (UST), the required energy at the high-frequency is transmitted to the material's surface via a ball, shots, or multiple pins. Consequently, an innovative nano-crystallized surface is formed, which progressively enhances the mechanical properties, corrosion resistance, friction, and wear resistance [56]. As illustrated in Fig. 5, the ultrasonic system comprises multiple parts such as an ultrasonic wave creator, a transducer device, a sonotrode, and an impact tool [57]. The generator transforms the input current into electrical signals of high frequency, and the transducer transforms them into high-frequency mechanical vibrations. The ultrasonic transducer creates an amplitude that is enhanced by the sonotrode and sent to the tool. Finally, the working tool starts vibration at the costumed amplitude/frequency throughout the UST.

In contrast to other SSPD methods, UST-based techniques offer multiple benefits, including superior performance, reduced weight, exceptional precision, resource efficiency, and eco-friendliness. This has led to an increase in researchers' interest in this technology in recent years (Fig. 4c). Fig. 6 suggests a classification for surface processing techniques. It is observed the the most important SSPD techniques utilizing ultrasound waves are ultrasonic shot peening (USP), ultrasonic peening treatment (UPT), ultrasonic nanocrystalline surface modification (UNSM), ultrasonic impact treatment (UIT), ultrasonic cold forging technology (UCFT), ultrasonic surface burnishing (USB), and ultrasonic deep cold rolling (UDCR) [56].

The ultrasonic-based SSPD processes can be categorized as USP, UPT, and USR techniques, the processes of which are schematically illustrated in Fig. 7. In USP, ultrasonically accelerated hard balls are directed towards the sample surface. The random impact of the balls causelocal plastic flow/ dimpling of the surface (Fig. 7a). The UPT utilizes hard pins/rods to impact the targeted surface towards enhancing its integrity/mechanical properties (Fig. 7b). In USR, the material surface is alternatively impacted by high-frequency impacts of a tool comprising a rotating ball (Fig. 7c) [56].

4.2.1. Ultrasonic shot peening (USSP/USP) processes

Peening, as defined by DIN 8200, is a mechanical technique used for surface processing/hardening of materials [58]. USSP, also referred to as SMAT, relies on the impact of hard spherical (steel) balls on the component's surface, using ultrasonic energy. The balls (usually 1-3 mm in diameter) are situated in a reflecting chamber that is shaken by a vibration generator (Fig. 8a). The chamber is capable of generating vibrations at frequencies ranging from

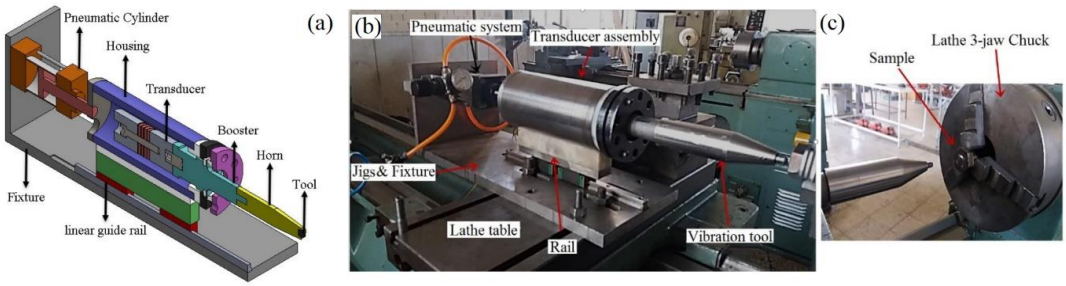

Fig. 5- Equipment for ultrasonic impact treatment on a lathe: (a) schematic illustration of the ultrasonic generator, (b) overall view, and (c) detailed view of the sample [57].

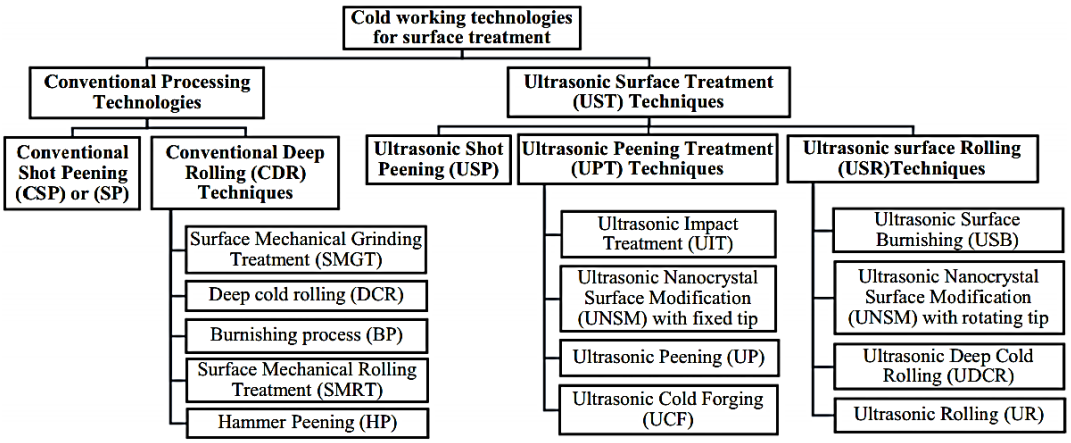

Fig. 6- Classifications of surface treatment cold working technologies [56].

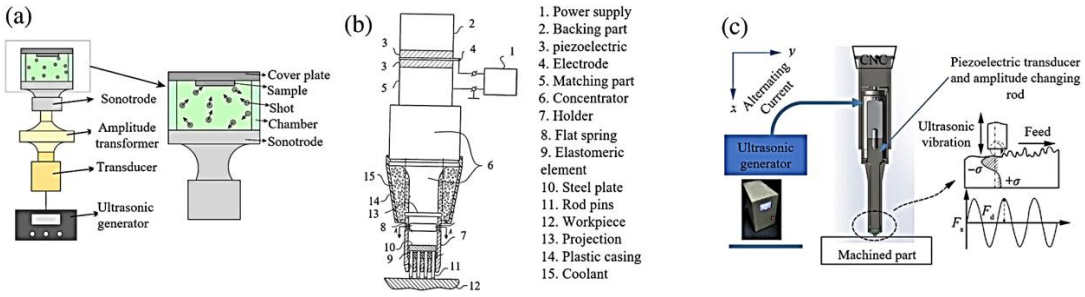

Fig. 7- UST techniques based on cold working: (a) USP; (b) UPT; (c) USR [56].

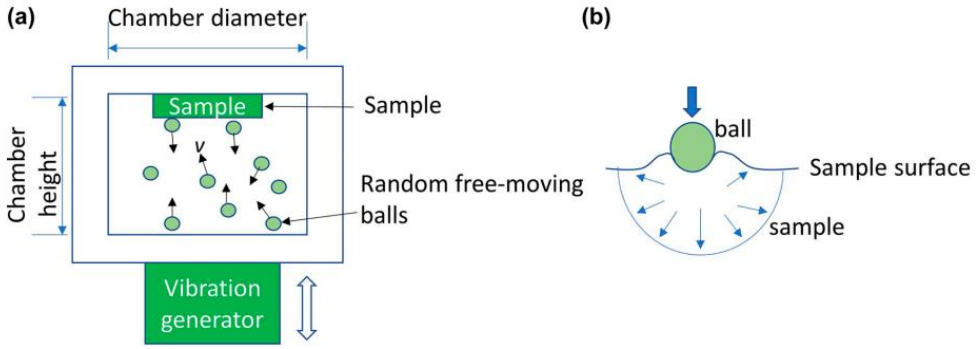

Fig. 8- Schematic depiction of USSP (a) procedure and (b) mechanics of deformation [62].

50 Hz to 20 kHz [55,59-61]. When the balls are resonated, the sample's surface is randomly struck by numerous flying balls in a short period of time. Every impact causes plastic deformation in the surface of the sample at a high strain rate, leading to significant plastic deformation (Fig. 8b) and gradual grain refinement throughout the entire surface down to the nanometer scale [59]. The main advantage of this method is that a low surface roughness is attained due to using high-quality shots and reduced impact velocity [59-62].

This method finds numerous industrial uses, including aerospace, maritime and shipbuilding, automotive, railway, and bridge engineering, where materials require exceptional strength, fatigue endurance, and corrosion and wear resistance. It has been widely employed to produce ultrafine/nanocrystalline surfaces in low-carbon steel [63], Cu [64], Al [65], Mg [66] alloys, in addition to stainless steel [67-69] and Ti [70], where certain severe plastic deformation techniques like ECAP require significant loads and specialized dies. The USSP is applicable for specimens with intricate geometries. However, during this process, the surface is impacted by an erratic and forceful projectile, leading to less uniformity compared to alternative methods, and typically, comprehensive surface coverage is hard to attain. Consequently, it is essential to choose the process parameters to achieve the desired surface roughness and maintain consistent surface coverage [71]. Alternatively, brittle fracture and surface wrinkling in the deformed layer during shot peening may happen and exacerbate corrosion and crack development [72].

4.2.2. Ultrasonic impact treatment (UIP)

A variation of the USP, the UIP, uses steel pins on an impact head that is attached to the tip of an ultrasonic sonotrode (Fig. 9). The pins get kinetic energy from the vibrating ultrasonic sonotrode tip, and the hits that follow on the surface being treated provide vertical force. Shear force may be generated when the pinhead rotates around the sonotrode axis [55].

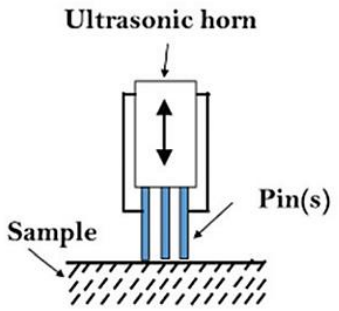

Fig. 9- Workflow of the UIP [55].

4.2.3. Ultrasonic peening treatment (UPT)

The UPT method, recognized as a highly promising cold surface treatment technique for metallic materials, was initially developed by Mukhanov and Golubev during the 1950s. In 1960, Krylov and Polischuk suggested a round shot located between the target surface and the ultrasonic transducer that induced significant plastic deformation. In 1970, Estatnikov created an ultrasonic magnetostrictive oscillating system featuring a peening tool, subsequently using the method to enhance the quality and dependability of welded joints in rail and tubular structures. Later in 2006, he asserted that UPT was the optimal technique for enhancing large plastic deformations and improving fatigue strength [73-75].

In UPT methods (UPT, UIT, UCF, and UNSM with a fixed tip), high-frequency waves are transmitted to the surfaces of metallic materials via several pins or rods for grain size reduction, microstructural enhancement, geometric alterations, reduction of TRSs, and enhancement of fatigue strength/life. Superficial microcracks are likewise forged due to plastic deformation resulting from the peening [56,73,74]. The UIP method finds numerous industrial applications, including aerospace, marine and shipping, automotive, railway, and bridge infrastructures, where materials require exceptional strength, fatigue resistance, corrosion resistance, and wear resistance [73,74].

4.2.3.1. Ultrasonic impact treatment (UIT)

The UIT was initially suggested in 2001 by Piyon as a secure, efficient, eco-friendly, and straightforward SSPD technique [76]. In the UIT, electrical energy is transformed into high-frequency ultrasonic vibration pulses (20–55 kHz), which are transmitted to the target surface through a specifically designed hard tool, producing a highly deformed surface layer [77]. During this process, a large amount of the energy used is directly transformed into vibrations, lowering energy usage. This not only reduces CO_2 emissions but also cuts energy expenses for industries [76]. The UIT is employed to enhance the strength and extend the service life of engineering alloys by surface nanostructuring/densification, removing surface residual tensile stresses, and applying beneficial compressive stresses [78]. This technique is commonly applied in aerospace, automotive, shipbuilding, and several other sectors to enhance materials' fatigue life, hardness, and corrosion resistance [76].

4.2.3.2. Ultrasonic nanocrystalline surface alteration (UNSM)

During the UNSM process, a WC tip or Si_3N_4 ball, propelled by an ultrasonic horn, impacts

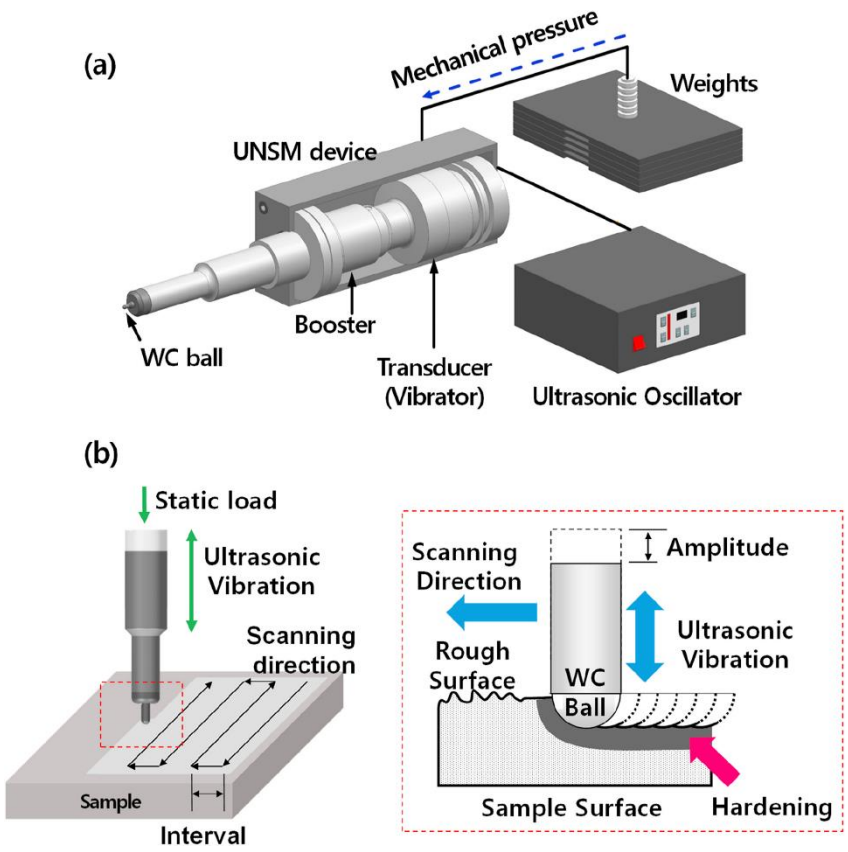

Fig. 10- Schematic representation of UNSM (a) configuration and (b) process concept [80].

the specimen surface and continues to move horizontally at a steady feed rate [62]. The UNSM has been utilized to improve surface characteristics by creating gradient variations in the grain refinement of a material's surface. UNSM equipment comprises an ultrasonic generator, an air compressor, a control card, and a guiding unit (Fig. 10). The ultrasound transducer powers the UNSM, generating tens of thousands to millions of mechanical ultrasonic waves each second. Nonetheless, since the ultrasound transducer produces only a few micrometers of amplitude directly, an acoustic horn is often utilized to amplify the amplitude. The intensified mechanical ultrasonic wave is then utilized to propel a tip ball, causing it to hit the target material's surface and produce significant surface plastic deformation on the specimen. Relative to the UIT, the UNSM offers numerous benefits, such as reduced energy usage and the implementation of static loading in surface treatment, guaranteeing consistent processing [79].

Currently, researchers have noted that UNSM can be effectively utilized for a variety of materials, including various steel grades [81-83], Al alloys [8485], Ti alloys [86,87], Mg alloys [84], Cu alloys [84], shape memory alloys [84], Ta [88], high entropy alloys [84], and superalloys [84,89,90].

4.2.3.3. Ultrasonic cold forging method (UCFM)

The UCFT is a novel, user-friendly, and eco-friendly technology that employs ultrasonic vibration energy to cause significant plastic deformation on metal surfaces. The UCFT transforms the material surface structure into a nanocrystal configuration extending to a specific depth, lowers surface roughness to 0.08–0.5 μm, enhances mechanical properties, wear, and fatigue performance, and creates surface CRS [91-93]. Fig. 11 illustrates the design and concept of the UCF apparatus. It comprises multiple parts including an ultrasonic generator (a) that generates electric ultrasonic frequency, an air compressor (b) which drives an ultrasonic generator unit, a $Pb(Zr,Ti)O_3$ piezo-transducer (c), a booster (d) that enhances the ultrasonic vibrations, a horn (e) that conveys the ultrasonic vibrations, and a WC ball tip (f) [94,95].

4.2.3.4. Rotating pins ultrasonic peening (RPUP)

The RPUP method employs rotating pins activated by ultrasonic vibrations to create intense plastic deformation in the surface and near-surface areas of metallic materials. Like other ultrasonic-based SSPD methods, RPUP seeks to improve surface material characteristics by introducing CRSs and altering the surface microstructure. A piezo-ceramic transducer located on the lathe carriage, an ultrasonic generator operating between 21 kHz and 0.6 kW, a stepped ultrasonic horn made of high-strength Ti alloy, and an impact head positioned at the horn's tip are all part of the RPUP configuration. The impact head has one or more cylindrical pins (width of 5 mm, length of 18 mm, mass of 3 g) that freely travel between the treated surface and the horn tip. Fig. 12 [96] displays the two types of impact heads utilized in this study.

For RPUP processing of flat samples, a seven-pin head (Fig. 12a) was rotated forcibly by an electric motor mounted on the transducer housing, and a unique system ensured the continuous adjustment of the head rotation speed. In this manner, the shear strain mode can be acquired during the impact of a pin on the surface of the sample. This feature, together with the lathe carriage's assistance in moving the acoustic system around the surface, causes the surface to produce multidirectional effects. The one-pin head is used to manufacture the round bar samples, which are held at both ends by a three-jaw spindle chuck and tailstock utilizing a collet chuck (Fig. 12b). In this case, the rotation of the sample itself and the continuous movement of the complete auditory system appear to have achieved the shear strain mode [96]. Regarding Fig. 12c, the basic concept of the RPUP for flat surfaces can be summarized as follows: line A-B is gradually moved along by the acoustic apparatus with a rotating head that has pins oscillating between the ultrasonic horn tip and the surface being treated. Then, it is moved transversely to point C and then back along the line C-D. This process is repeated until the full target surface area has been treated. Compared to USP or SMA procedures, which use high-energy balls to randomly strike metallic components, it appears that the RPUP approach offers more control [96].

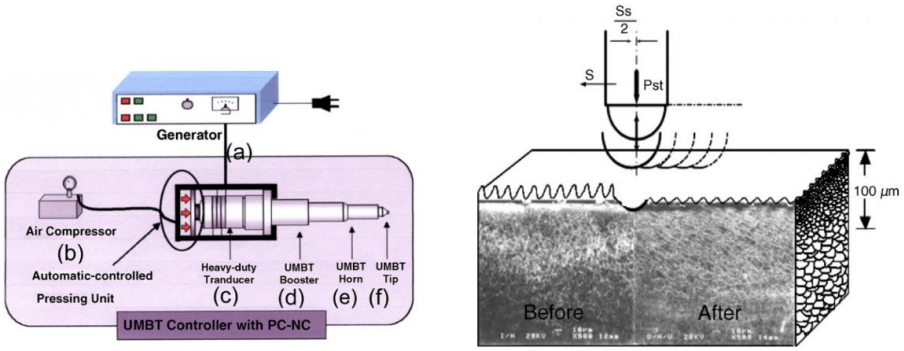

Fig. 11- Configuration and the process device of the UCFT [94].

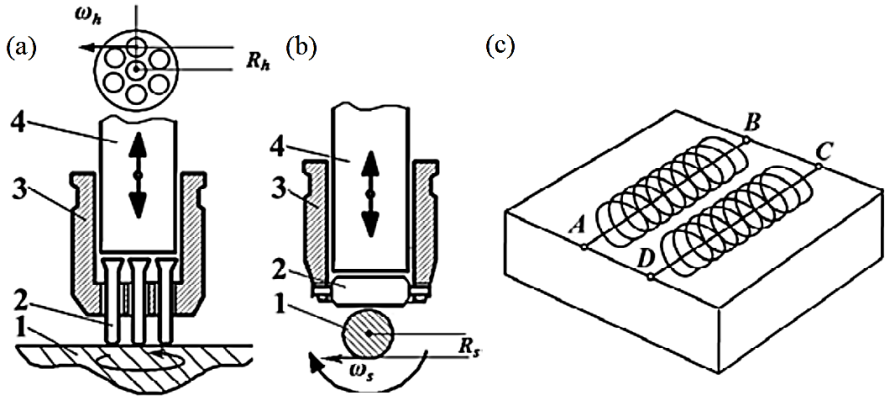

Fig. 12- Impact heads used for RPUP processing of flat (a) and round-bar (b) specimens: (1) specimen, (2) pin(s), (3) head body, (4) ultrasonic horn (sonotrode). ωh, ωs and Rh, Rs denote the head/sample linear velocities at rotation and their respective radii, (c) the fundamental concept explanation of the RPUP method (general view of the processed sample) [96].

4.2.4. Ultrasonic surface rolling (USR) techniques

The USR technology, known for its distinct, clean, and debris-free shaping process, is extensively used for surface strengthening of different metals [97]. In the USR methods, the target surface is directly influenced by the impacts of a rolling ball/roller tool under extremely high frequency. This creates an ultrafine/nanocrystalline micro-dimpled microstructure on the surface, enhancing the mechanical, tribological, and fatigue resistance of the material [56,98].

4.2.4.1. Ultrasonic surface rolling treatment (USRT), Ultrasonic surface rolling process (USRP), and surface ultrasonic rolling treatment (SURT)

As proposed by Wang et al. in 2008, the USRP is an innovative and effective technology for surface modification, integrating UIP and deep rolling (DR) processes. In the USRP process, the simultaneous influence of the static force and ultrasonic vibration on the target material's surface (Fig. 13) caused by the rolling ball tip leads to significant plastic deformation of the surface, ultimately producing a gradient nanostructured (GNS) layer that measures several hundred micrometers. USRP can also smooth the surface roughness of the target material, as the plastic flow generated during this process levels off the peaks of the material surface into the troughs, essentially resulting in peak clipping and valley filling [55].

In addition, the beneficial residual compressive stress is imposed on the surface of workpiece. Reducing surface roughness can prevent the onset of microcracks, while the development of a GNS layer and residual compressive stress can hinder crack growth, resulting in the USRP-treated material exhibiting enhanced surface mechanical properties [97,99-103]. USRP is capable of forming nanostructured surface layers, enhancing mechanical properties, and fatigue strength and wear resistance across various metals [104-106].

Currently, researchers have reported that USRP technology can be effectively utilized for various materials, including multiple grades of steel [101,107,108], Al alloys [99,109-111], Ti alloys [112-114], Mg alloys [106,115], Cu alloys [116,117], high entropy alloys [118], W heavy alloys [119], and even superalloys [120,121].

4.2.4.2. Ultrasonic deep cold rolling (UDCR)

In UDCR, dynamic loading is layered over static loading, resulting in the local absorption of ultrasonic energy, which alters the metal flow conditions and alleviates strain. The incorporation of dynamic stress into the amplitude of static stress creates a total stress high enough to surpass the dislocation of potential barriers, thereby prompting an earlier onset of plastic flow. Moreover, the dislocation density in the material rises once plastic deformation occurs, leading to an increase in the microhardness of the modified surface.

A unique device was created and established for executing the UDCR process. It comprises a WC ball (6 mm in diameter) featuring a Dymon-IC coat to minimize friction and withstand high-speed impact forces during operation, a piezoelectric transducer with piezoceramic rings for generating ultrasonic vibrations, an ultrasonic generator that produces high-frequency ultrasonic energy at 20

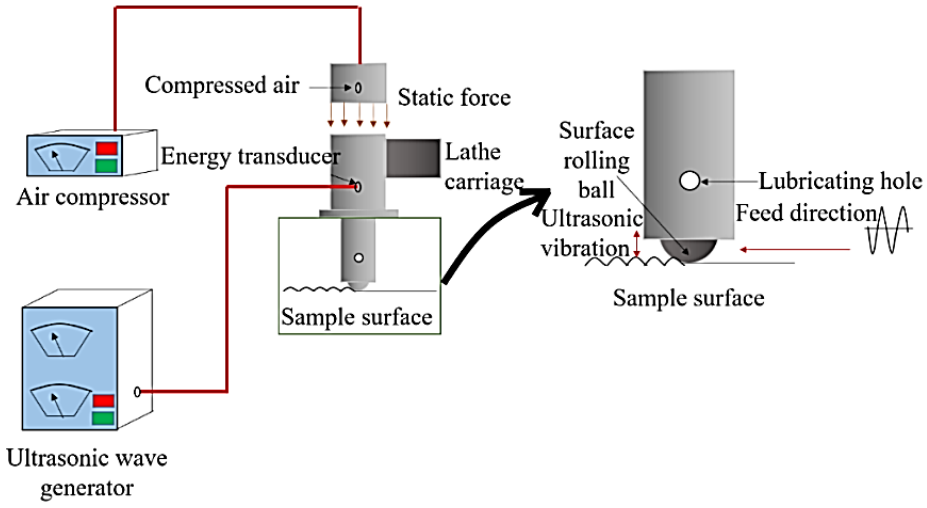

Fig. 13- Schematic diagrams showing the fundamental working process of USRP [106].

kHz, and a pressing mechanism to exert a static force, ensuring continuous contact between the ball and the surface of the part being treated. Fig. 14 illustrates the experimental configuration and the fundamental principles of the UDCR process [122-124].

4.2.5. Ultrasonic abrasion finishing (USAF)

The USAF is a sophisticated polishing method that can complete the finishing of AMed components. Material removal from the surface takes place as a result of low-amplitude, high-frequency vibrations of the tool against the material's surface when fine abrasives are present. This technique reduces the surface roughness by 129 μm/min facilitates a removal of 3 to 4 μm in 2 seconds, and ultimately achieves a final roughness ranging from 0.3 to 0.8 μm. Based on the vibration direction (Fig. 15), the USAF method is classified into three distinct techniques [125].

4.2.6. Ultrasonic vibration-supported ball burnishing (UVABB)

During the UVABB process, a supplementary vibratory and/or ultrasonic motion is introduced alongside the tool's forward motion, which results in the tool having a reciprocating displacement. Therefore, contrary to conventional burnishing (CB) methods, implementing ultrasonic displacement leads to a well-uniformed surface integrity, improves the stiffness of the contact, enhances the lubrication retention, and enhances the tribological properties. It is worth noting that the distinction between the CB and UVABB lies in their vibration frequency. The vibration frequency of the former ranges between 20 and 50 Hz, while in the latter it ranges in kHz. Fig. 16 illustrates the design of the ultrasonic vibration wing tool [125].

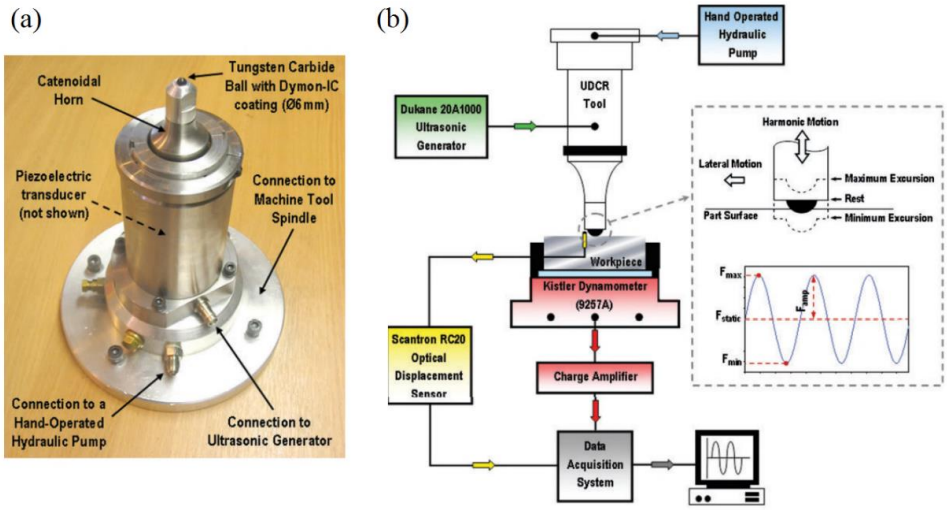

Fig. 14- (a) Apparatus and (b) schematic principle along with experimental arrangement for the UDCR process [123].

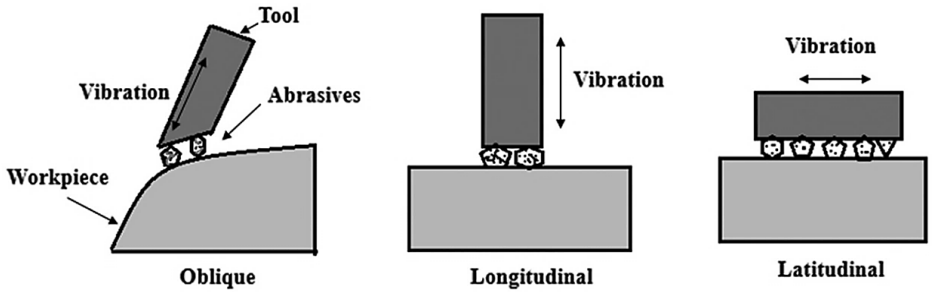

Fig. 15- Schematic diagrams illustrating the methods of finishing through USAF [125].

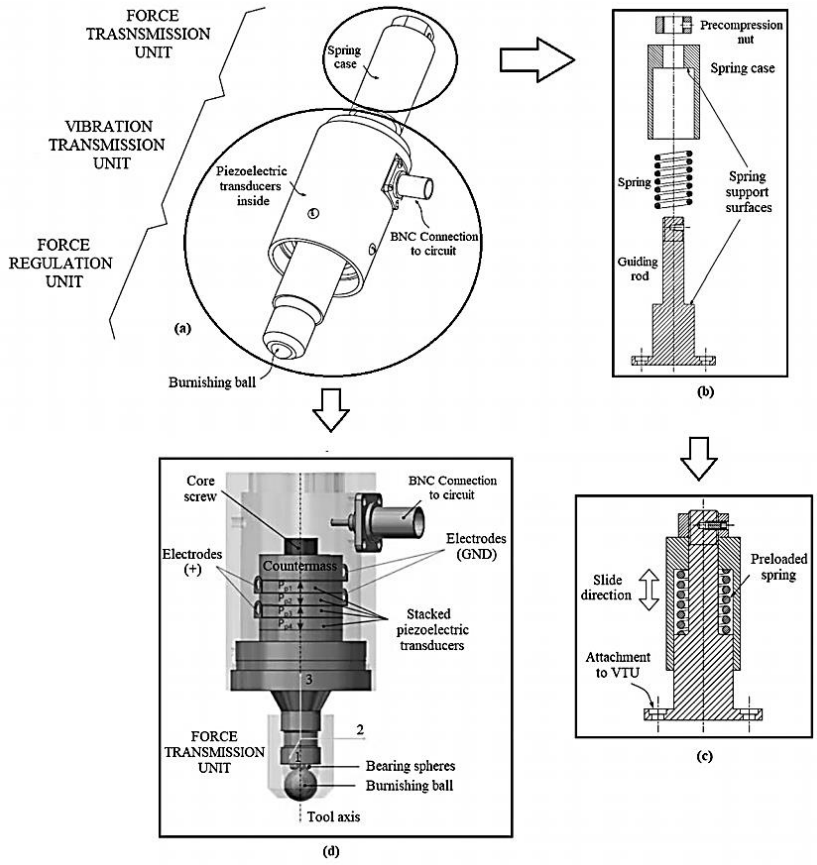

Fig. 16- (a) Shematic diagram of the UVABB device, (b) components of the load transfer unit, (c) elements of the vibration transfer, and (d) elements of the force transfer unit [125].

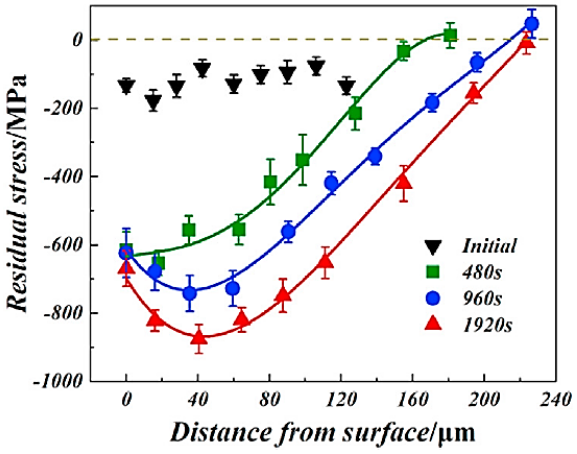

Fig. 17- The distribution of residual stress with varying USP durations [126].

5. An overview of ultrasonic-based SSPD post-processing methods for SLMed parts

As discussed previously, SLMed metallic materials suffer from drawbacks such as low surface quality (roughness), the development of surface TRSs, and the large extent of surface/bulk porosities. These issues harm the performance of SLMed components in service conditions. In the following, the most common ultrasonic-based post-processing techniques, comprising ultrasonic shot peening, ultrasonic peening, ultrasonic rolling, and other (less common) processes capable of alleviating the above-mentioned issues will be discussed.

5.1. Ultrasonic shot peening post-processing

Ultrasonic post-processing techniques based on shot peening are designed to be used on complex parts with finalized geometry. Accordingly, these techniques rank among the most popular post-processing techniques for SLMed components, and extensive research has been published to optimize the tools and process variables for better SLMed part performance. The impact of USP on the surface characteristics and morphology of SLM parts has been the subject of a large percentage of these studies. For instance, Zhang et al. [126] explored how USP influences the microstructure of the SLMed Ti-6Al-4V alloy sample. Their findings indicated that both hardness and induced compressive stresses rose with longer USP time, with the effective hardening depth measuring approximately 0.3 mm. A 25% increase in surface hardness was also noted. They also found that extending the peening time leads to an increase in the CRS at both the surface and bulk of the samples (Fig. 17).

X-ray diffraction (XRD) analysis revealed that as the USP time increased, the diffraction peaks broadened (Fig. 18), which signifies increasing microscopic strains and a reduction in crystallite size. The XRD results also showed that the samples' microstructure consists of α-phase throughout the USP process, with no new phase being formed [126].

In another research work, Alharbi [127,128] studied the influence of USP on the surface texture and roughness of a SLMed 316 stainless steel. It was figured out that utilizing USP with a power of 600 W for 15 minutes using a ball diameter of 6 mm and a gap distance of 30 mm, as the ideal parameters, results in a surface roughness of 7.47 μm and a surface hardness of 411 HV, demonstrating a reduction of approximately 176% and an improvement of around 90%, respectively.

Regardless of surface integrity, many studies have investigated/analyzed the effect of USP processing on the corrosion, wear, and mechanical/fatigue characteristics of SLMed parts. For example, Xu and colleagues [129] also showed that USP can enhance the surface and wear characteristics of 316L SLMed components. After 1 min and 3 min of USP, the R_a value reduced by 35 and 45%, respectively compared to the unprocessed sample. The EBSD results also indicated that applying the USP for 1 and 3 minutes substantially refined the surface/subsurface grains and increased the corresponding nano-hardness values by 29 and 32%, respectively. The wear tests also revealed the positive impact of the USP on the wear depth.

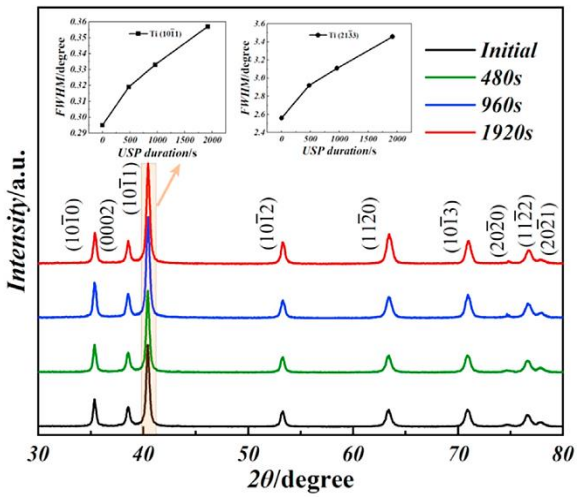

Fig. 18- XRD examination of the surface layer in SLMed Ti-6Al-4V alloy, prior to and following USP treatment, showing peak broadening in USPed samples [126].

In Yu et al.'s work [130], the influence of USP on the surface structure and mechanical characteristics of a SLMed Ni-based superalloy (GH3230) was investigated. The USP test conditions were established as follows: one hundred SAE52100 hardened steel balls (3 mm in diameter) with an amplitude of 45 μm and a frequency of 20 kHz. The samples underwent the USP for 240, 300, 360, and 840 seconds. Their results indicate that USP for 840 seconds produced a defect-free layer approximately 330 μm thick on the surface and resulted in aUFG microstructure (Fig. 19). USP also generated surface compressive stresses (Fig. 20a), notably enhanced the surface hardness (Fig. 20b), and improved the yield strength, ultimate tensile strength, and elongation by 24.1%, 8.6%, and 18.2%, respectively, in comparison to the annealed sample (Fig. 20c-20d).

Srikanth et al. [131] studied how USP influences the electrochemical corrosion resistance, high-temperature oxidation, and hot corrosion resistance of Ti6Al4V alloy produced by the SLM process. Their findings indicated a marked improvement in electrochemical corrosion resistance in 3.5 wt% NaCl solution, elevated temperature oxidation resistance, and hot corrosion resistance in Na_2SO_4 + 25 % NaCl and Na_2SO_4 + 50 % V_2O_5 at 750 °C following the USSP treatment.

Yan et al. [132] utilized ultrasonic SMAT to alter the surface microstructure of SLMed Ti6Al4V ELI and enhance its fatigue life. They demonstrated that the SMAT technique can create a nanostructured surface on SLMed samples by rapid applied strains. This layer enhances the mechanical properties of the SMAT-affected zone and generates CRS at the surface, thereby inhibiting crack formation. Consequently, following SMAT, the sample shows markedly greater fatigue strength compared to the untreated (SLMed) specimen in both low- (675 MPa vs 350 MPa) and high-cycling regimes (580 MPa vs 290 MPa) (Fig. 21).

To enhance the tensile properties of SLMed 316L stainless steels, Portella et al. [133] utilized SMAT processing. The process was executed at low intensity (treatment duration of 10 min, 2 mm shot size of 100Cr6, and Almen intensity of 0.14 mmA) and high intensity (treatment duration of 30 min, 3 mm shot size, and Almen intensity of 0.19 mmA) at a consistent frequency of 20 kHz. The results are presented in Table 1. SMATed samples exhibit enhanced mechanical characteristics based on the treatment intensity.

Kan et al. [134] also showed the beneficial effects of SMAT processing on the surface nano-crystallization/hardening of SLMed 316L stainless steel. Ghosh et al. [135] attempted to enhance the tensile properties of SLMed 316L samples through SMAT treatment. According to their findings, the SMATed sample has a functional microstructure after a nanostructured surface layer. As the SMAT duration grows from 15 to 60 minutes, the depth of the processed gradient layer progressively increases from 20 to 40 μm, with no further changes beyond 60 minutes of the processing time. As seen in Fig. 22, they also investigated the ductility and yield strength of 316L stainless steel specimens treated using different techniques. SLMed material treated by SMAT exhibits a superior strength-to-ductility ratio compared to conventional micro-crystalline, bulk nanostructured, and high-performance SS 316L.

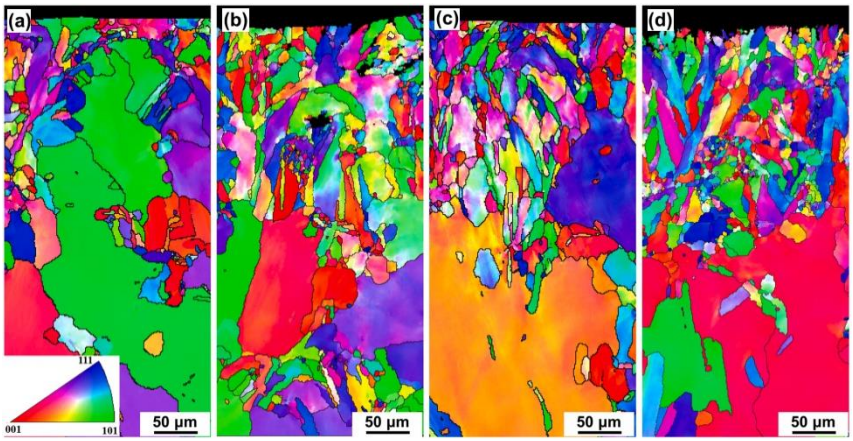

Fig. 19- Inverse pole figure of Ni-based SLMed samples subjected to various treatments: (a) USP-240 s, (b) USP-300 s, (c) USP-360 s, (d) USP-840 s [130].

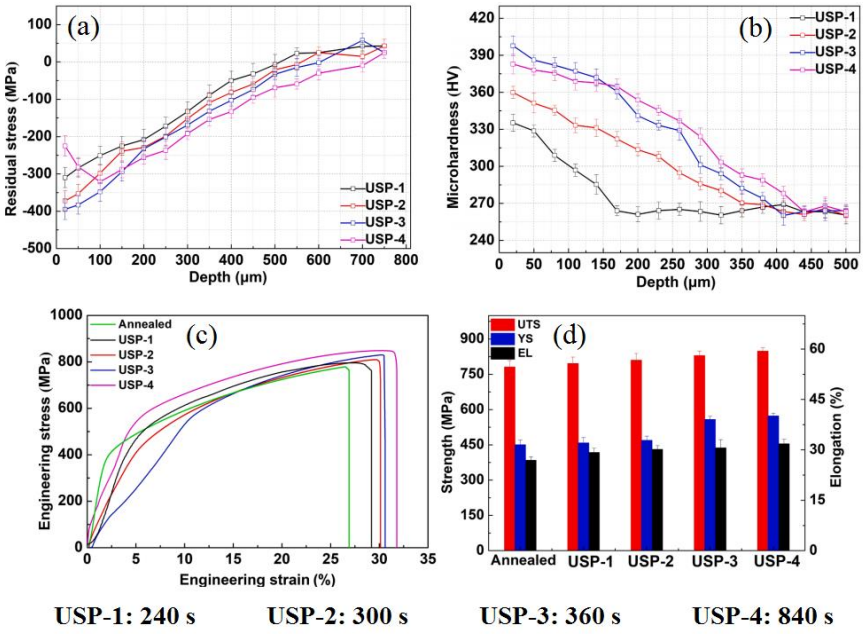

Fig. 20- (a) Distribution of residual stress, (b) microhardness profile, (c) engineering stress-strain graphs, and (d) tensile mechanical characteristics of GH3230 samples exposed to various USP durations [130].

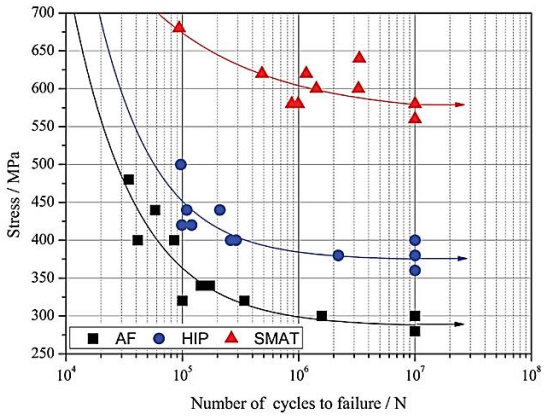

Fig. 21- S-N curves for the fatigue specimens (AF: as-fabricated, HIP: hot isostatic pressed, and SMAT) [132].

Table. 1- Mechanical characteristics acquired from as-received and SMATed 316L samples [133].

	As-received	SMAT low	SMAT high
Elongation (%)	29 ± 3	22 ± 0.4	16 ± 2
Difference from the unprocessed sample (%)		−24	-45
Yield strength (MPa)	527 ± 767	599 ± 0.5	624 ± 16
Difference from the unprocessed sample (%)		+14	+18
Ultimate tensile strength (MPa)	611 ± 5	669 ± 2	676 ± 13
Difference from the unprocessed sample (%)		+9	+11

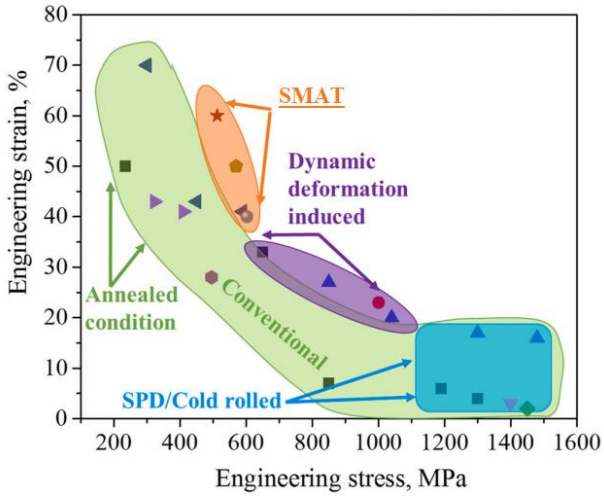

Fig. 22- Comparison of yield strength versus elongation for different 316L stainless steels produced by different routes[135].

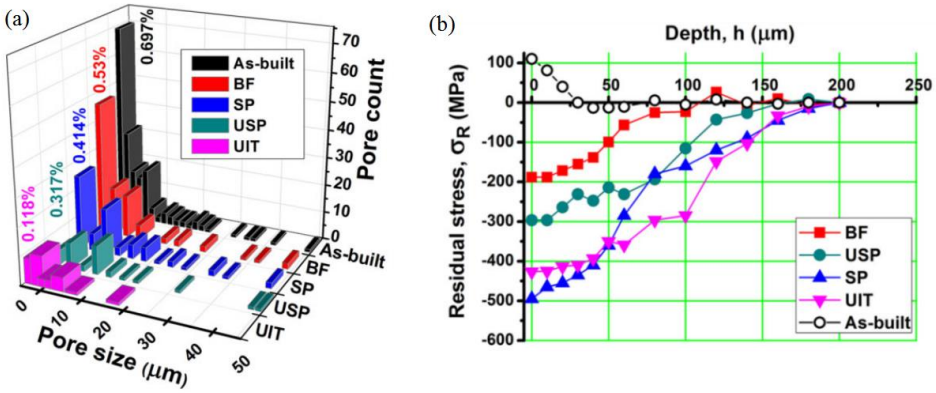

Fig. 23- (a) Relative porosity and (b) residual stress depth profiles formed in the build direction of the SLMed and BF, SP, USP, and UIT processed IN 718 specimens [136].

The comparison between the effects of the USP and other SSPD processes on the microstructure and properties of SLMed parts is presented as follows. Lesyk et al. [136] examined the influence of BF, SP, USP, and UIT processes on the porosity level and residual surface stresses in SLMed Inconel 718 alloy. As illustrated in Fig. 23a, the BF, SP, USP, and UIT processes caused the porosity values to decrease by 23.1, 40.6, 55, and 84%, respectively, compared to the residual porosity of the SLM-constructed specimen (0.697%). The UIT procedure substantially decreased the amount of microporosities at the surface region (0.118%). The tensile stresses of the SLM-made specimen (+120 MPa) were effectively transformed into compressive stresses through the application of the BF (−201.4 MPa), USP (−313.8 MPa), multi-pin UIT (−428.7 MPa), and SP (−510.7 MPa) methods (Fig. 23b).

Zhang et al. [137] also analyzed and compared the impact of pneumatic shot peening (SP) and USP at an Almen intensity of 0.2 mmA on the microstructure and corrosion resistance of the SLMed Ti64 alloy. The average surface roughness (R_a) of the SPed sample measured 1.806 μm, considerably exceeding the values of the USPed samples (0.942 μm and 0.999 μm). Their findings indicated that the SP generated a reduced crystallite size and resulted in the highest surface and maximum CRS, measured at -654.0 MPa and -805.5 MPa, while the USP led to thicker layers of CRS. The USPed sample achieved the maximum microhardness (443.2 $HV_{0.025}$) and the thickest hardened layer (247.8 μm). The USP and SP led to

enhanced corrosion resistance; however, the USPed samples demonstrated high corrosion potentials and reduced corrosion current densities.

Also in an interesting study, to address the inherent low printability of Al alloys, Liu et al. [138] introduced an innovative hybrid AM method for processing Al-Mg-Sc alloy by integrating SLM with interlayer USP. They indicated that the interlayer USP depth reached approximately 700 μm, resulting in near-complete density (the porosity of the material reached 0.049% following the HAM treatment) (Fig. 24) and a shift in residual stress from tension to compression (Fig. 25a). The SLM with subsequent aging treatment reaches a yield strength of 609 MPa and fracture elongation of 7.5%, showing exceptional strength and decent ductility (Fig. 25b and 25c) in comparison to other Al alloys produced through AM and forging.

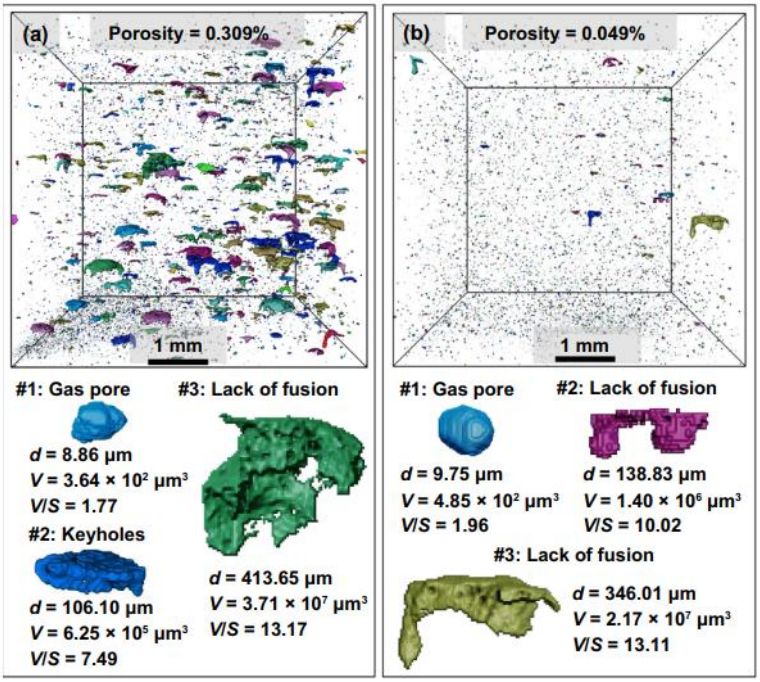

Fig. 24- Micro-CT scans displaying 3D distributions of defects and porosities in (a) SLMed and (b) HAM (hybrid AMed) samples [138].

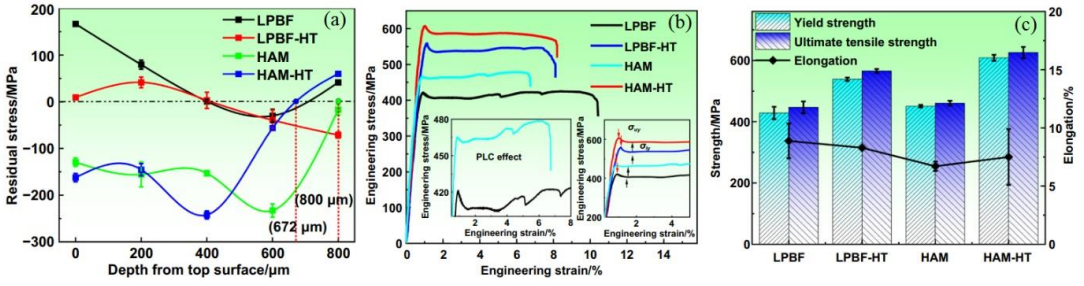

Fig. 25- (a) Distributions of residual stress and (b,c) tensile characteristics of as-SLMed and HAM (hybrid AMed) Al-Mg-Sc alloy samples [138].

5.2. Ultrasonic peening post-processing

Despite their unique features and capabilities, the application of USP techniques for SLM post-processing encounters significant limitations regarding the control of the velocity and direction of the shots, their impact positions on the target surface, and their full coverage. However, UPT is a promising surface technology which, due to its unique characteristics, does not usually encounter many of the above limitations. Based on that, considerable research works have been conducted on the UPT effect on the microstructure and properties of SLMed parts [139-144].

Ma and colleagues [145] showed that applying UNSM can smooth down the surface of SLMed NiTi by removing asperities, decreasing its average roughness from 12.1 to 9.0 μm. As observed in Fig. 26, the primary rough surface (Fig. 26a, 28b, and 26c) of the 3D laser printed metal transformed into a much smoother one (Fig. 26d, 28e, and 26f). During UNSM, the burnishing action eliminates surface particles, while the ultrasonic impact reduces the height of asperities by forging them into the valleys. This method leads to a significantly improved surface quality. Furthermore, enhanced wear properties, improved corrosion behavior, densified microstructure, and significantly increased surface hardness (from 300 to 400 HV) are noted.

Kim and his team [146] investigated the impacts of UNSM on SLMed M4 high-speed tool steel containing Mo and W. The study showed that UNSM effectively reduces surface roughness, changes tensile residual stresses to compressive stresses, and greatly enhances the surface hardness and wear resistance of SLMed M4 steel.

Moreover, Kim et al. [80] demonstrated that employing UNSM on laser-based directed energy deposition 316 stainless steel components resulted in a surface waviness of 1.8097 μm and a roughness of 0.3297 μm, reflecting enhancements of 80% and 72%, respectively, when compared to the untreated specimen. UNSM notably refined the material grains (Fig. 27) and greatly raised the amount of martensite, leading to a surface microhardness increase of up to 71.2% (Fig. 28).

Zhang et al. [147] indicated that UNSM can markedly enhance the fatigue strength of LPBFed Ti64 (Fig. 29). Besides improved surface quality and reduced porosity content, it was seen that the TRSs initially developed in the as-received samples changed to CRSs (Fig. 30). The combined influence of improved surface integrity, low porosity content, high hardness, and beneficial CRSs led to a notable enhancement in fatigue life.

The study of Ma et al. [148] suggested that UNSM can effectivelyreduce surface porosity, enhancing fatigue strength, corrosion resistance, and wear resistance, as well as transforming surface tensile stresses into surface compressive stresses in laser 3D-printed components. Ma states that the UNSM treatment lowers the R_a of the SLMed Al-10Si-Mg alloy from 0.5 to 0.06 μm (~88% reduction) and decreases the wear rate by about 85%.

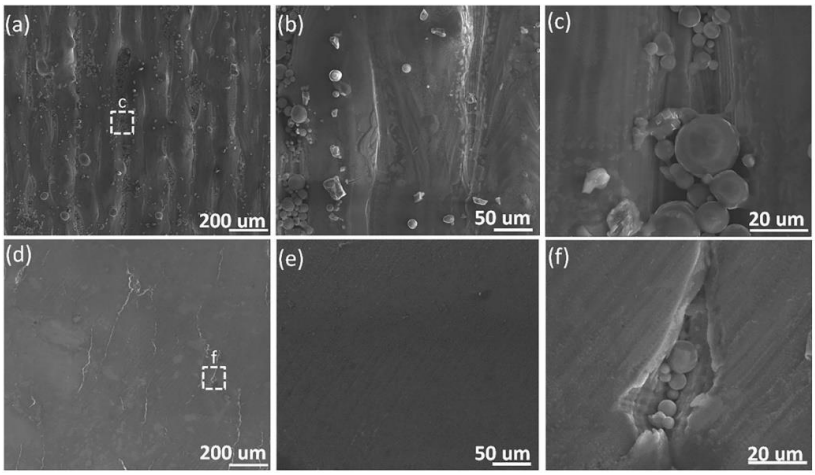

Fig. 26- SEM images showing the surface morphology of (a, b, and c) as-SLMed and (d, e, and f) UNSM-treated NiTi samples [145].

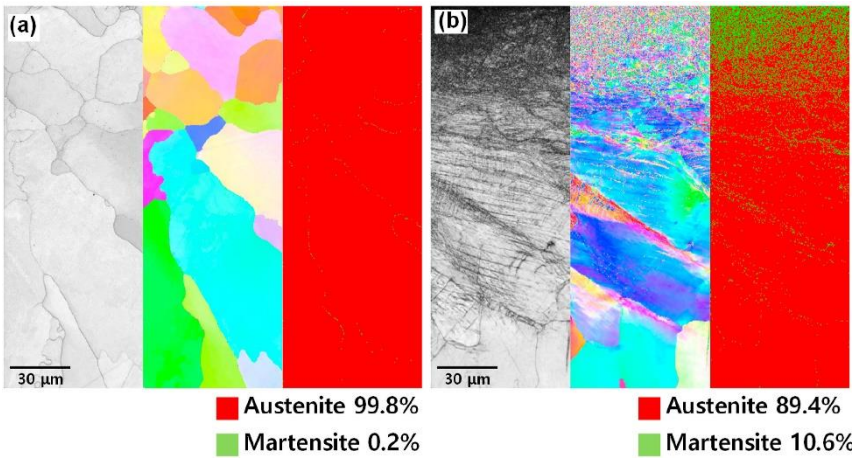

Fig. 27- SEBSD analysis of the near-surface microstructures (a) prior to and (b) following UNSM treatment [80].

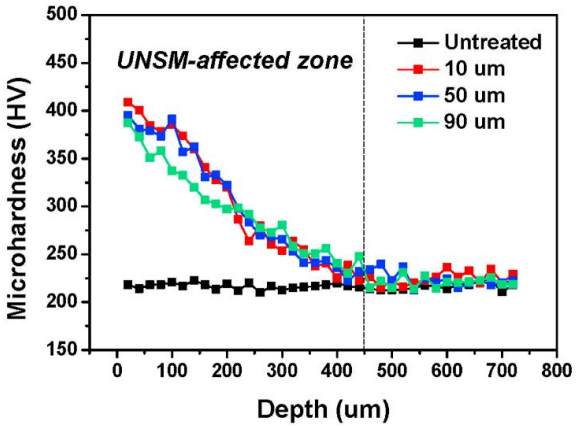

Fig. 28- Variation of microhardness with depth from the surface following the UNSM on laser-based directed energy deposition 316 stainless steel components [80].

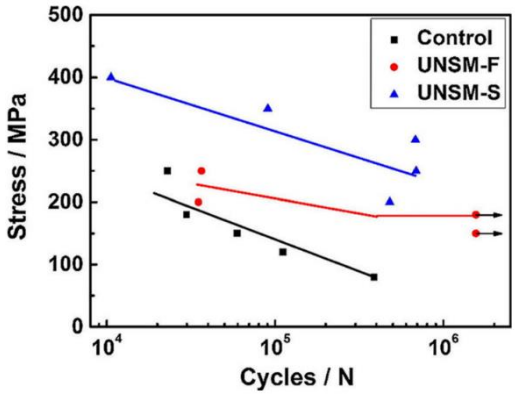

Fig. 29- S–N curves from rotational bending fatigue experiments of LPBFed Ti64 prior to and following UNSM treatment [147].

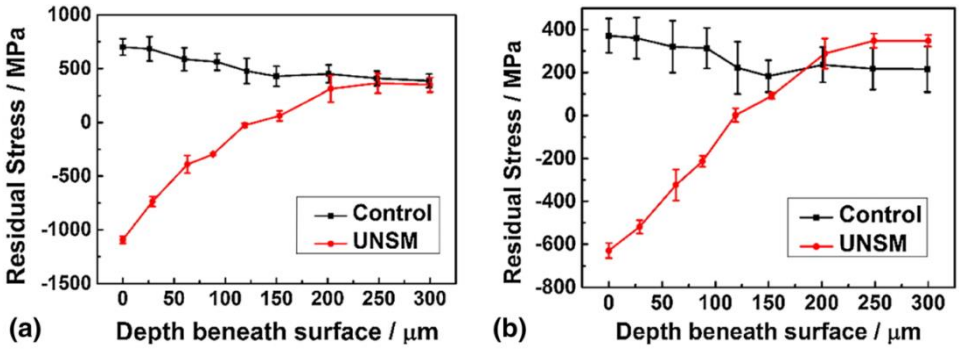

Fig. 30- Detailed RS profile of LPBFed Ti-6Al-4V samples in the UNSM (a) transverse direction and (b) scanning direction prior to and following process [147].

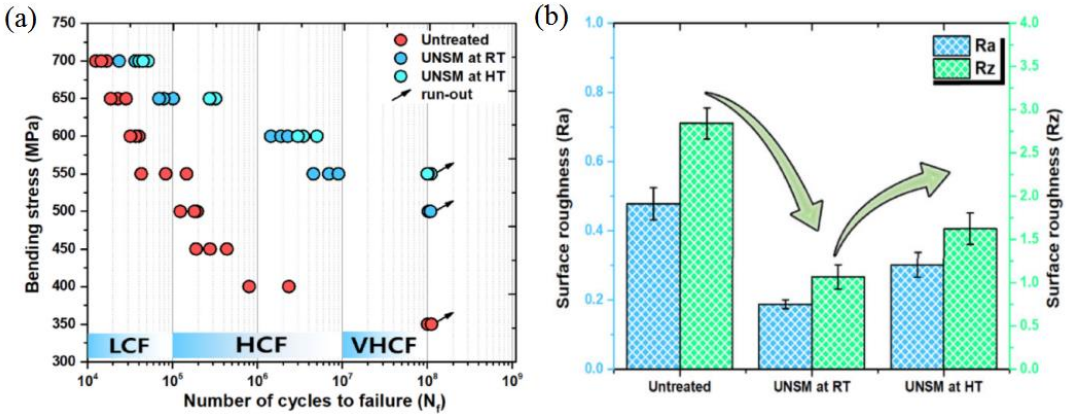

Fig. 31- Comparison of (a) S–N data and (b) surface roughness for untreated and UNSM-treated Inconel 718 samples at room and high temperatures [149].

Karimbaev et al. [149] investigated the impact of UNSM treatment at both room temperature and elevated temperatures (RT and HT) on the fatigue behavior and mechanical characteristics of IN718 produced through direct energy deposition (DED). At RT and HT, the UNSM treatment notably enhanced the fatigue performance by around 43% and 57%, respectively (Fig. 31a). This is attributed to the formation of a nanostructured surface layer and the development of a high CRS. According to Fig. 31b, following UNSM treatment at RT and HT, the surface roughness of the untreated sample significantly lessened, which is vital for avoiding the initiation of surface fractures. A close analysis of the worn surfaces revealed that the main fracture initiation point for the UNSM-treated samples occurred at the subsurface, whereas for the untreated samples, it was at the upper surface. A crack initiation site was relocated into the subsurface through the application of a high CRS via UNSM treatment at RT and HT.

Amanov et al. [150] investigated the effects of the UNSM process temperature on the mechanical and tribological characteristics of CoCrMo alloy in another study. R_a and R_z values of 8.484 and 43.505 µm, respectively, dropped to 1.440 and 12.435 µm, as well as to 1.044 µm and 7.644 µm following UNSM at ambient and high temperature, indicating a noticeably rough surface profile in the as-received specimen (Fig. 32a).

Additionally, the surface hardness of the as-received specimen was increased from about 37 HRC to about 56 and 66 HRC, respectively, following UNSM at room and high temperatures (Fig. 32b). It was also observed that applying the UNSM at room and high temperatures, caused an increase in the proof and tensile strengths of the alloy from about 630 to 652 and 705 MPa and from about 707 to 746 and 784 MPa, respectively. The average COF (0.0959) after UNSM at room and high temperature was also dropped to 0.0735 and 0.0498, respectively (Fig. 33a). Moreover, following the UNSM at room and elevated temperatures, the wear rate dropped from 5.47 to 3.12 and 1.24 $mm^3 \times 10^{-12}$/N×m, respectively (Fig. 33b).

Attempts have also been made to improve the UNSM effectiveness. For instance, Zhang et al. [151] tried to improve the UNSM performance by applying a direct current to the SLM-fabricated Ti6Al4V specimen. The process was conducted at a static load of 30 N, ultrasonic vibration amplitude of 24 µm, a frequency of 20 kHz, and a scanning speed of 2000 mm/min. It was found that the direct electrical current maintained the processing sample temperature at about 426°C, causing a more effective surface improvement where the R_a decreased from 10.6 to 1.3 µm and hardness augmented from about 360 to 485 HV.

In another research work, Amanov et al. [152] investigated the separate and composite effects of laser shot peening (LSP) and UNSM on SLMed Ti–6Al–4V samples. According to their findings, following the LSP, the surface R_a value of the as-fabricated specimen was augmented from about 9.96±0.90 to about 12.10±1.04 µm. However, after receiving UNSM treatment, it drastically decreased to 1.07±0.06 µm. Although still higher than that of the sample treated with UNSM alone, applying the LSP followed by UNSM and UNSM followed by LSP again decreased the R_a to 1.53±0.25 and 1.60±0.11 µm, respectively. The samples treated with UNSM and LSP had surface hardness values of 352.0 HV and 343.3 HV, respectively (Fig. 34a). Moreover, compared to the samples processed by LSP+UNSM (364 HV), applying UNSM followed by LSP caused a rather higher surface hardness of about 367 HV. Applying LSP followed by UNSM also led to a change in surface RS from tensile to compressive state, where the greatest CRS value (-705 MPa) was obtained. Importantly, the subsequent LSP treatment helped to mitigate the CRS brought on by UNSM treatment (Fig. 34b).

The tribological test results also revealed a significant reduction in the wear and friction of Ti-6Al-4V samples. For instance, the wear rate dropped from about 3.5 to about 2.1 $mm^3 \times 10^{-7}$/Nm in the UNSM+LSP sample (Fig. 35). Compared to both unprocessed and LSPed samples, the LSP followed by UNSM and UNSM followed by LSP also dramatically decreased the COF.

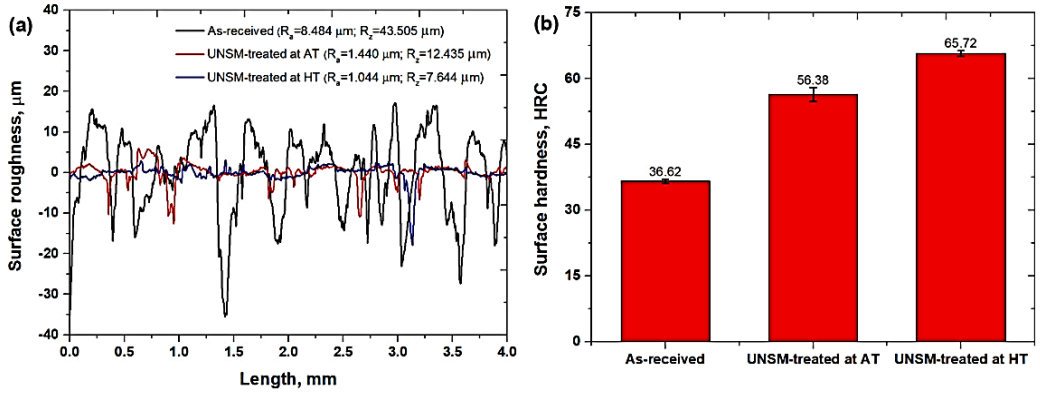

Fig. 32- (a) Surface roughness and (b) surface hardness of the as-received and UNSM-treated CoCrMo specimens at ambient temperature (AT) and high temperature (HT) [150].

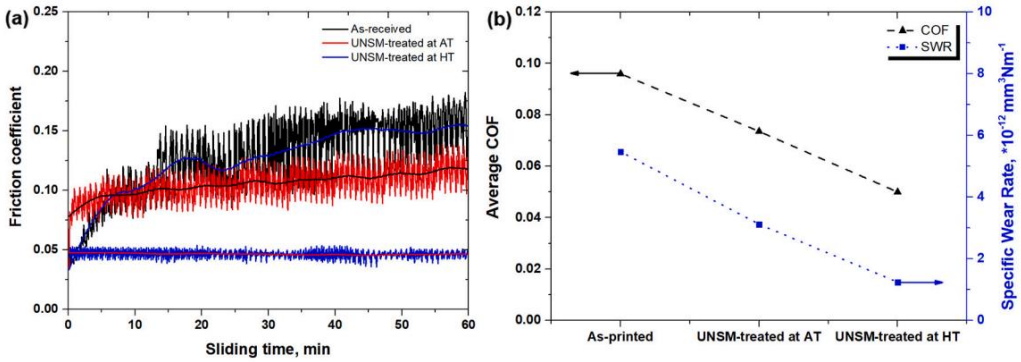

Fig. 33- Variation of (a) friction coefficient against the sliding distance and (b) average friction coefficient and specific wear rate of the as-received and UNSM-treated CoCrMo specimens at ambient temperature (AT) and high temperature (HT) [150].

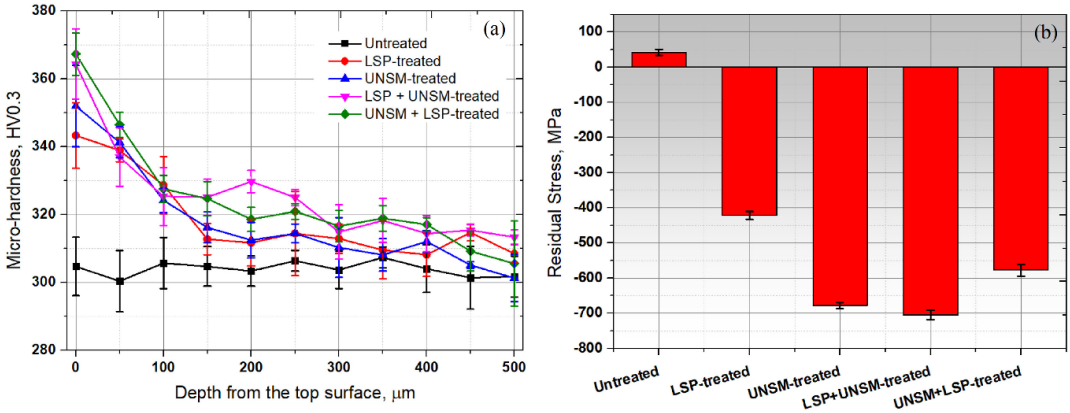

Fig. 34- Variation of (a) microhardness below the processed surface and (b) surface RS of the un-processed, LSPed, UNSM-treated, LSPed + UNSM-treated, and UNSM-treated + LSPed SLMed Ti-6Al-4V samples [152].

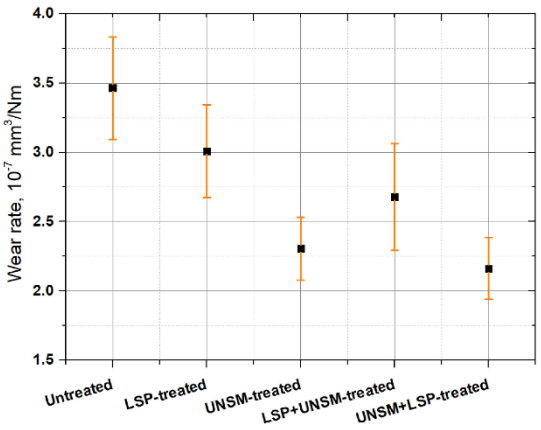

Fig. 35- Wear rates of the as-received, LSPed, UNSM-treated, LSPed + UNSM-treated, and UNSM-treated + LSPed SLMed Ti-6Al-4V specimens [152].

As previously mentioned, despite some advantages of the UNSM process over UIT, such as higher energy efficiency and greater consistency, these processes are very similar in terms of equipment and process principles. Recently, some researches have been conducted on the effect of UIT on the surface properties of SLMed parts, and significant results have been obtained. For instance, Ansarian et al. [43] described how multi-pass UIT affects the microstructure, mechanical properties, and tribological features of a SLMed commercially pure Ti (CP-Ti). UIT significantly improved the acicular martensites formed after SLM process and achieved a uniform and dense surface microstructure, leading to a decrease in porosity content of 1-, 3-, and 5-pass UITed samples by 43, 60, and 67%, correspondingly. The nanoindentation findings for the 3-pass UITed sample showed an increase of approximately 53, 45, and 220% in its nanohardness, H/E_r, and H^3/E_r^2 metrics, respectively. The R_a and R_{sk} in the three-pass UITed sample were found to be smaller than those of the SLMed sample by 95% and 223%, respectively. At typical pressures of 0.05 and 0.2 MPa, the wear rate and friction coefficient of the 3-pass UITed sample were reduced compared to the SLMed sample by 65 and 58%, and 20 and 17%, respectively.

Ansarian et al. [153] likewise validated the beneficial effect of UIT on the corrosion characteristics of SLMed CP-Ti, observing that its corrosion current density reduced from 4.8 to 0.72 μA/cm^2 following a 3-pass UIT. Nonetheless, an additional increase in UIT passes was indicated to impair the corrosion resistance due to the development of surface microcracks and the spallation of the oxide layer (Fig. 36).

Liu et al. [154] applied the UIT as a post-treatment technique to the SLMed Haynes 230 alloy. Results indicate that UIT can successfully seal pores, with the internal porosity of the UIT-treated layer decreasing by 63.6%, 70.9%, and 81.8% after one, two, and three applications, respectively. Additionally, the UIT reduced the strength of the texture and improved grain refinement, particularly encouraging the development of fine grains. Additionally, the ultimate tensile strength and yield strength of the best impact process rose by 9.6% and 34.6%, respectively. The typical friction coefficient decreased by 4.9 %–14.6%. Xing et al. [155] examined the influence of UPT on the stress corrosion resistance of SLMed AlSi10Mg parts. They demonstrated that UPT significantly enhanced surface hardness and transformed the residual stress from a tensile state to a compressive state to a depth of approximately 1.5-2 mm. UPT further decreased the porosity of SLMed samples. These effects led to an enhancement in the stress corrosion behavior of the samples.

Fig. 37 illustrates the corrosion plots of the as-manufactured samples prior to and following the UPT in a 3.5% NaCl solution. As shown in Fig. 37a, the polarization curves of the specimen before and after the UPT were quite alike, suggesting nearly identical corrosion levels regardless of the UPT procedure. A comparison of the two curves reveals that at a given corrosion current density, the corrosion potential of the UPTed specimen was greater than that before the UPT. Nevertheless, there was no considerable change in the corrosion currents in the as-received (4.59×10^{-8}) and UPTed sample (5.26×10^{-8}). In the UPTed sample, the E_{corr} was found to be about −0.486 V higher than that of the as-received sample, with a deviation of 44 mV illustrating the positive impact of the UPT on the stress corrosion behavior of the SLMed samples.

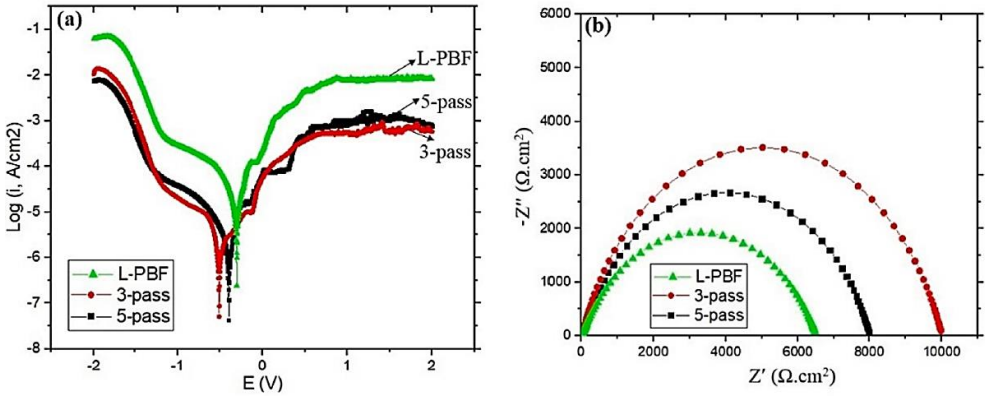

Fig. 36- (a) Tafel polarization graphs and (b) Nyquist diagrams of CP-Ti specimens in As-LPBFed and UITed conditions [153].

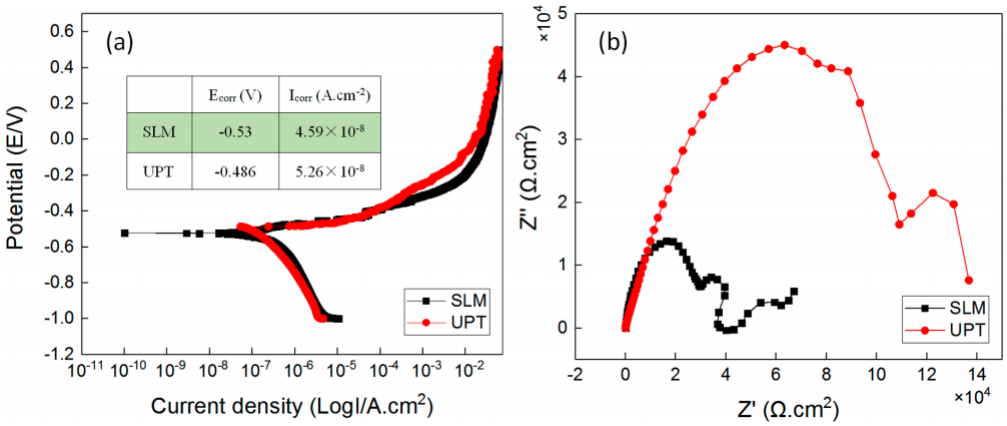

Fig. 37- The effect of UPT on stress corrosion characteristics of SLMed Al-10Si-Mg alloy (a) Polarization graph; (b) EIS Nyquist plot [155].

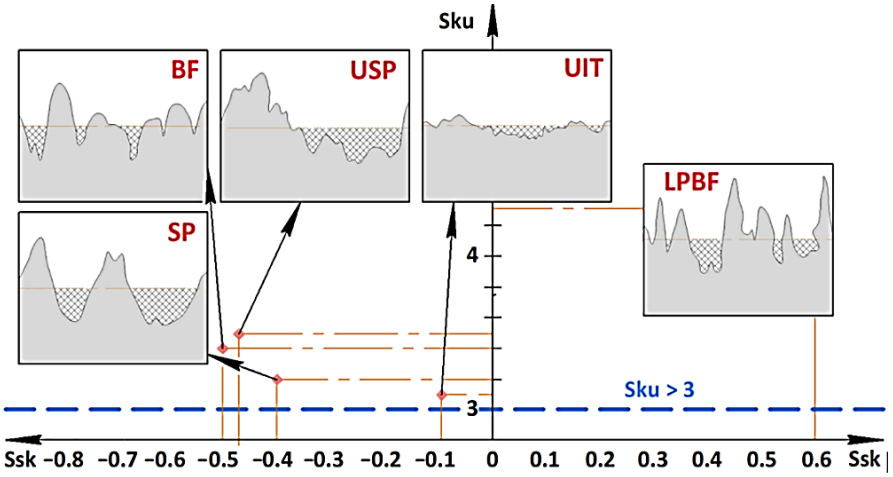

Fig. 38- Maps of skewness and kurtosis accompanied by surface profiles of the SLMed and BFed, SPed, USPed, and UITed IN718 samples [156].

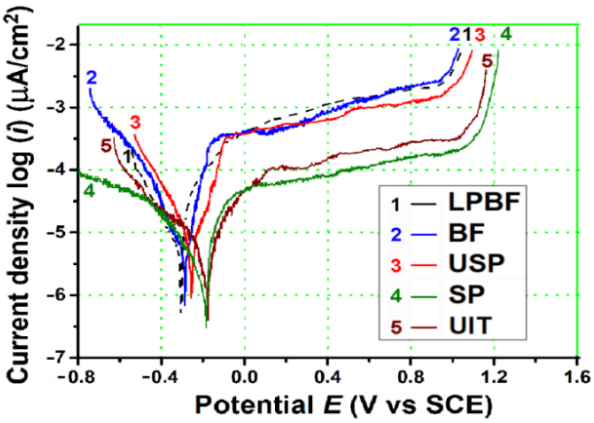

Fig. 39- Potentiodynamic polarization graphs for the SLMed and mechanically surface-finished IN 718 alloy specimens following BF, USP, and SP [156].

The Nyquist results (Fig. 37b) also reveal that the UPT has the potential to improve the corrosion resistance of SLMed Al-10Si-Mg samples, [155].

In a comprehensive and applied study, Lesyk et al. [156] compared the effects of UIT, USP, SP, and barrel finishing (BF) techniques on the surface specification/surface integrity of SLMed IN718 alloy. Based on their results, the efficiency of the processes was ordered in this ascending sequence: BF, USP, and UIT/SP. The suitable surface enhancement technique can be chosen according to the surface criteria, hardening level, depth of hardening, crystallite dimension, residual stress (RS), and average surface roughness. BF is mainly applicable for the surface finishing of intricate SLMed IN718 alloy (hardening intensity level of about 6.5%, depth of hardening equal to 100 μm, crystallite dimension of approximately 34 nm, RS = −200 MPa, and mean surface roughness of 2.68 μm). USP post-processing (hardening intensity level of about 13.5%, depth of hardening of 140 μm, crystallite dimension of about 23 nm, RS = −315 MPa, and mean surface roughness of 0.75 μm) is quite manageable and adaptable, yet USP can be used solely for surface quality improvement and hardening of small and intricate SLMed parts. Conversely, multi-pin UIT post-processing (hardening intensity level of about 25.5%, crystallite dimension of approximately 15 nm, depth of hardening equal to 200 μm, RS = −430 MPa, and mean surface roughness of 0.33 μm) is advisable for the surface quality enhancement of large SLMed components featuring straightforward shapes. SP post-processing (hardening intensity level of about 42%, depth of hardening equal to 200 μm, crystallite dimension of about 10 nm, RS = −510 MPa, and mean surface roughness of 1.68 μm) is an effective post-processing technique (corrosion rates are nearly seven times reduced following the SP treatment compared to the SLMed IN 718 alloy sample) which may be utilized for surface quality enhancement of large- and small-sized SLMed components [156].

Fig. 38 displays the Skewness-Kurtosis maps and surface roughness profiles of the experimental samples. Surface finishing led to kurtosis (S_{ku}) values of about 3, indicating the formation of a uniform distribution of peaks and valleys throughout the surface. The S_{sk} values declined toward lower values following the application of surface finishing. The improved surface profile of the UITed specimens is anticipated to enhance tribological and corrosion behaviors, as the S_{sk} approached 0, suggesting an even distribution of peaks and valleys. In contrast to the UITed alloy, the SP- and USPed samples exhibited higher amounts of deep pits on their surfaces. Moreover, in contrast to the SLMed specimen, the surface asperities were smoothened, signifying negative values of the S_{sk} in the surface-processed samples [156].

As seen in Fig. 39, the polarization plots of the post-processed SLMed samples showed increased potentials (E) and reduced corrosion densities, indicating the surface-treated samples corroded at a significantly slower rate compared to the SLMed sample. In comparison with the BFed sample with a corrosion potential of −96 mV and the USPed sample with a corrosion potential of −291 mV, the SPed and UITed samples exhibited high corrosion potential. The corrosion potentials were −199 mV and −197 mV in SPed and UITed samples, respectively.

Building on their earlier work, Lesyk et al. [156] analyzed the wear and friction characteristics of the as-fabricated and ultrasonically treated SLMed Inconel 738 samples. Their findings indicated that UIT is the most efficient technique for enhancing wear performance. The SLMed samples exhibited a wear resistance of (5.57×10^{-2} μm^{-1}), which was significantly improved by UIT (6.76×10^{-2} μm^{-1}, 121% compared to SLMed) and USP (5.89×10^{-2} μm^{-1}, 106% compared to SLM) techniques.

5.3. Ultrasonic rolling process (USRP)

Another common type of ultrasonic-based SSPD process is surface rolling using ultrasonic vibrations. Below, some of the most recent and important research on the effect of this process on the characteristics and surface properties of SLMed parts is reviewed.

Yang et al. [157] utilized USRP to increase the surface finish and corrosion resistance of SLMed 316L stainless steel. The results demonstrate a significant improvement in the surface quality and corrosion resistance of 316L stainless steel. Surface roughness was reduced by 82.46%, peak residual compressive stress achieved ~800 MPa, and microhardness rose notably by 48.15 $HV_{0.5}$. Under a static pressure of 550 N, the USRP-treated sample demonstrated the best corrosion resistance, showing a decrease in self-corrosion current density of around 36%, which resulted in a significant enhancement in corrosion resistance.

Chen et al. [158] examined the effectiveness of USRP technique in forming a ~300 μm gradient nanotwinned structure on the surface of a SLMed CoCrNi medium-entropy alloy. It was indicated that the yield strength and 10^7-cycle fatigue endurance limit were notably enhanced by the USRP, reaching increases of 192 MPa and approximately 130 MPa, respectively. They ascribed the enhanced fatigue characteristics to several factors that collectively inhibit crack initiation from the sample surfaces, such as the existence of a gradient nanotwinned layer and a decrease in irregular defects found on and below the surface.

Xu et al. [159] utilized the USRP to enhance the surface corrosion resistance of 316L stainless steel produced by SLM. Their findings showed that after the USRP, the samples achieved reduced surface roughness (up to 95%), enhanced microhardness (up to 53%), compressive residual stress (up to -212 MPa), and a decreased grain size (approximately 16%). At a static pressure of 200 N, the USRPed sample exhibited the highest corrosion resistance, with the corrosion current density dropping by as much as 41%, the polarization resistance rising by 34%, and the donor and acceptor densities decreasing by approximately 51 and 81%, respectively. This enhancement was associated with the altered surface roughness, refined grain structure, higher Cr_2O_3 levels in the passive film, work hardening, and compressive residual stresses.

Wang et al. [160] examined the influence of USRP and direct current-assisted USRP (DC-USRP) on the block-on-ring wear characteristics of SLMed Ti-6Al-4V alloy. In comparison to the as-built (4×10^{-5} $mm^3N^{-1}m^{-1}$) and USRPed samples (5×10^{-6} $mm^3N^{-1}m^{-1}$), the findings showed that the DC-USRPed sample exhibited the lowest wear rate of 1×10^{-6} $mm^3N^{-1}m^{-1}$ (Fig. 40a). The COF decreased with time in a manner consistent with changes in the wear rate (Fig. 40b). Owing to the changed lubrication mechanism, increased hardness, and higher CRS, the samples treated with USRP and DC-USRP exhibited improved wear resistance.

Liu et al. [161] invented a hybrid process of ultrasonic rolling and LMD (LMD-UR) to enhance the corrosion resistance of AMed 316L stainless steel. The LMD-UR samples exhibited better corrosion resistance than those made only using LMD. Fewer and smaller corrosion pits were noted on the surface of the corroded LMD-UR samples, while the LMD samples showed larger pits. The enhanced corrosion resistance of the LMD-UR alloy is due to the smaller size and lower fraction of pores, the fragmentation and uniform distribution of Cr-enriched ferrite phases, and the creation of a dense passive film encouraged by closely packed grain boundaries.

Liu et al. [162] examined the influence of USRP on the surface integrity, surface microstructural features, hardness, and RS of SEBMed Ti64 featuring an as-built surface. Findings indicate that simultaneous application of ultrasonic impact and static load improved the surface quality through flattening of the partially melted powders and the ridges/surface irregularities. Moreover, the sample's surface quality is notably enhanced, where the R_a and R_z were decreased by about 95 and 90, and the surface hardness was enhanced by approximately 16 % following the USRP. A hardened layer with a depth of more than 110 μm, having a gradient microstructure was achieved. Additionally, the surface wettability transitioned from hydrophobic to hydrophilic.

Qian et al. [163] examined the impact of the layer-by-layer USRP on the mechanical characteristics of selective laser melted AlSi10Mg alloy. Experimental findings indicate that the porosity drops to 1 %, exhibiting rather equiaxed grains (~ 8 μm). The formation of fine and equiaxed grains enhances the mechanical characteristics of SLMed alloys in the construction direction, raising the proof strength over 405 MPa, fracture strain to more than 8%, and compressive stress over 600 MPa (Fig. 41).

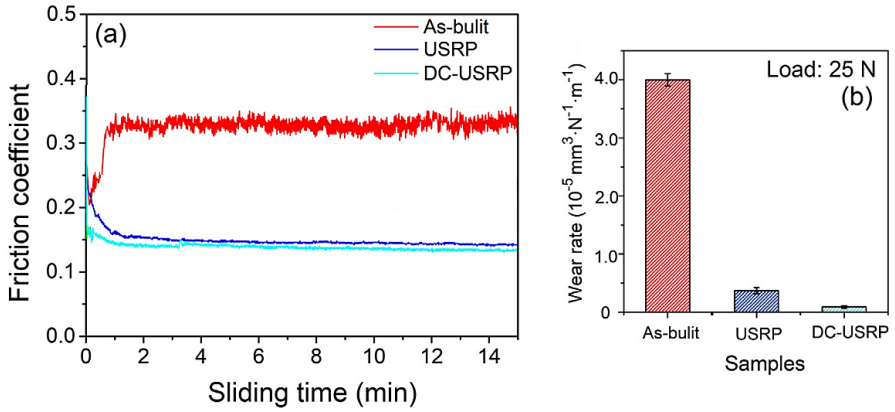

Fig. 40- (a) Coefficient of friction for SLMed Ti-6Al-4V samples subjected to USRP and DC-USRP (b) comparison of wear rates [160].

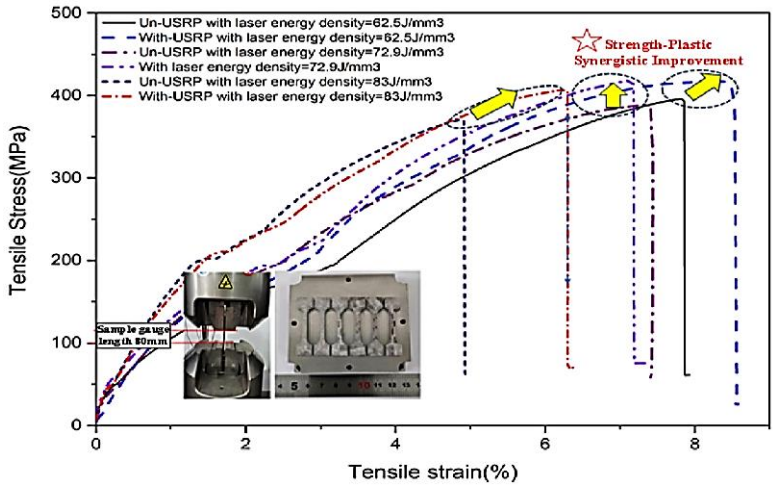

Fig. 41- Comparison of mechanical properties between as-printed AlSi10Mg samples and USRP tests: (a) engineering tensile stress-strain graphs [163].

5.4. Other ultrasonic-based SSPD processes

Appart from the more common processes discussed in previous sections, some ultrasonic SSPD methods have also been examined on a limited or case-by-case basis. Salmi et al. [164] introduced the ultrasonic-assisted ball burnishing (UABB) as an innovative method for surface quality enhancement of components produced by AM. Following the UABB the quality of the surface of CoCr parts (R_a = 0.18 µm) can be up to 32 times better than the as-received condition (i.e. R_a = 5.66 µm). Applying the UABB on 316L stainless steel parts also caused a decrease in the average roughness from 7.39 to 0.55 µm (about 13 times lower). Moreover, the UABB increased the hardness of CoCr and 316L components by 48% and 71%, respectively. Fig. 42 illustrates the elements subsequent to the UABB process.

In another research, Teramachi and Ian [166] employed the UABB technique to improve the surface quality of SLMed AlSi10Mg components. As illustrated in Fig. 43, unburnished surfaces exhibited uneven regions and cavities that resulted in a rough texture. Nonetheless, these uneven regions were significantly smoothed by the BB process, resulting in a 98% decrease in surface roughness and a 24% increase in hardness when compared to the as-SLMed AlSi10Mg component.

Ituarte et al. [167] also attempted to utilize the UABB as a post-processing technique for components produced by the LSM AM approach. They demonstrated that the application of the UABB process decreases the surface quality and enhances the hardness of a SLMed 18% Ni maraging tool steel. The R_a dropped from 6.24 µm to ~1.31 µm and lower, with the minimum value being 0.14 µm, contingent on process parameters. Moreover, in order to enhance surface integrity by reducing roughness and reconstructing microstructure, while optimizing fatigue performance and mitigating surface defects, Velázquez-Corral et al. utilized UABB [168]. These findings verify the beneficial effects of vibration-assisted ball burnishing over traditional ball burnishing on the roughness reduction and the enhancement of the depth of the affected subsurface.

Wang et al. [169] utilized ultrasonic abrasive polishing (UAP) to enhance the surface finish of SLMed parts. The collapse of cavitation bubbles in ultrasonic polishing has been shown to effectively eliminate partially melted structures, and additional enhancement in roughness can be achieved through micro-cutting and the impact of abrasive particles in the slurry (Fig. 44). This led to a decrease in roughness from 9.48 to 2.93 µm following 30 minutes of polishing.

Tan and colleagues [170] utilized ultrasonic cavitation abrasive finishing (UCAF) to process direct metal laser sintered (DMLSed) IN 625 specimens. In this process, bubble bursts on the target sample surface, resulting in surface erosion by which the surface irregularities are removed. The UCAF process can be utilized to diminish the surface roughness of workpieces, obtaining R_a values between 2.7 and 3.8 µm, irrespective of the initial surface roughness. The study revealed that the process performance was notable only for very rough surfaces during the initial phase

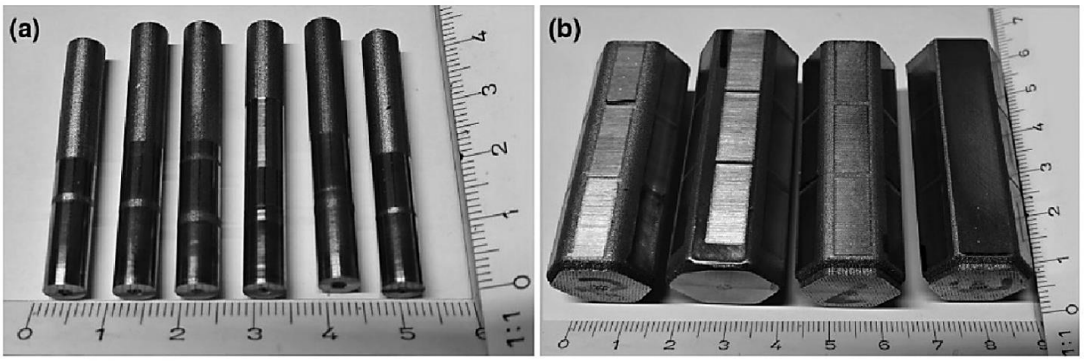

Fig. 42- (a) cylindrical CoCr components and (b) 316L stainless steel pyramids. Photos of the components post-UABB [165].

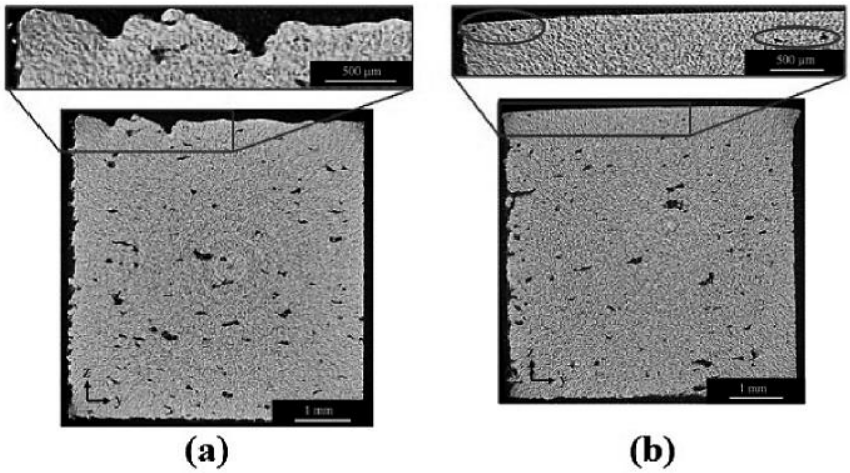

Fig. 43- Cross-sectional images of (a) un-burnished and (b) UVABB-treated SLMed AlSi10Mg samples [166].

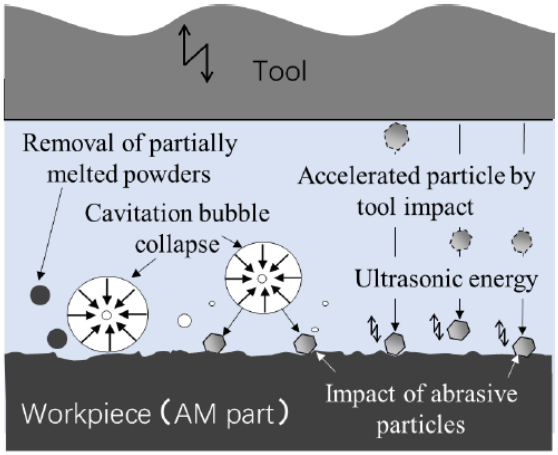

Fig. 44- Mechanism of material removal during UAP of components produced by additive manufacturing [169].

of machining. This change in the rate of material removal ensured dimensional precision for different surface types of all shapes. Additionally, the UCAF procedure strengthened the surface by 15%. The primary advantage of the UCAF procedure is that there is no contact between the machining head and the workpiece surface.

Cheng et al. [171] studied the impact of ultrasonic vibration-assisted compression (UAC) on the microstructure and hardness of SLMed stainless steel 316L. The UAC method integrates ultrasonic vibrations with the plastic deformation of the material [15,20]. Based on their findings, compared to the CC method, the true strain rose by 2.8% in the UAC method, demonstrating its effectiveness in reducing the forming stress of SLMed components. UAC was also shown to significantly enhance the number of sub-grain boundaries within the molten pool at the end surface, facilitating dislocation slip and grain refinement, with surface hardness increased by approximately 7% in comparison to the CC specimens (Fig. 45).

6. Overview and future outlook

AM commonly referred to as 3D printing, is significant because it provides design flexibility, facilitates quick prototyping and on-demand manufacturing, minimizes waste and expenses, and can result in lighter, more robust components. It also aids in the unification of assemblies, fosters customization, reduces supply chain risks, enhances part dependability, and provides support for AI-based design. SLM is regarded as one of the most adaptable additive manufacturing (AM) methods, especially for metals, because of its capacity to create intricate shapes and customized microstructures. It is capable of the formation of complex designs and integrated assemblies that are challenging or unfeasible to produce using conventional manufacturing techniques. Additionally, SLM decreases material waste and diminishes the requirement for thorough post-processing.

Although SLM offers design flexibility and allows for the creation of intricate shapes, it has several disadvantages, including rough surfaces, residual tensile stresses, porosity and internal defects, as well as microstructural segregation/inconsistencies that require post-processing. As we understand, material failure frequently begins at the surface. Consequently, post-processing techniques based on severe plastic deformation on surfaces have drawn the researchers' interest. In this study, it was attempted to explore the principles and effectiveness of several important processes, specifically ultrasonic-based surface severe plastic deformation methods in altering the structure and surface characteristics of components made by the SLM technique. The key processes analyzed were ultrasonic shot peening (USP), ultrasonic surface mechanical attrition treatment (SMAT), ultrasonic peening (UP), ultrasonic nanocrystalline surface modification (UNSM), ultrasonic impact treatment (UIT), ultrasonic rolling process (USRP), ultrasonic cold forging technology (UCFT), ultrasonic-assisted ball burnishing (UABB), and ultrasonic deep cold rolling (UDCR), ultrasonic abrasive polishing (UAB), ultrasonic cavitation abrasive finishing (UCAF), and ultrasonic vibration-assisted compression (UAC).

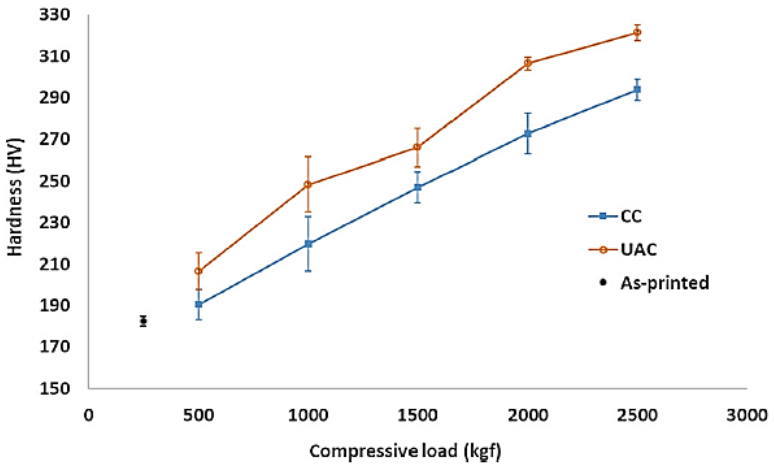

Fig. 45- Effect of ultrasonic vibration-assisted compression on the hardness of SLMed stainless steel 316L [171].

The investigations on different alloys, such as carbon steels, tool steels, stainless steels, Al alloys, Ni- and Co-based superalloys, and Ti and its alloys, demonstrate that applying these processes effectively enhances the surface microstructure, mitigates micro-segregations by breaking up the segregated regions, promotes UFG/nanocrystallization, increases microstructural densification, reduces surface roughness, alters tensile surface residual stresses to compressive surface stresses, and consequently leads to notable improvements in surface mechanical properties, fatigue strength, corrosion resistance, and tribological characteristics.

Future advancements in the ultrasonic surface post-processing of SLMed components will probably concentrate on enhancing efficiency, automation, standardization, and process optimization to improve efficiency and scalability. These might consist of robotic systems equipped with sophisticated sensors and algorithms for precise and efficient processing, integrating post-processing stages directly into the printing operation, and acknowledging attempts to streamline processes, standardizing equipment, and enhancing user interfaces to facilitate the integration of SLM and post-processing into manufacturing workflows for companies

References

1. Talebi M, Razaghian A, Saboori A, Niroumand B. Effects of Cu addition and heat treatment on the microstructure and hardness of pure Ti prepared by selective laser melting (SLM). Journal of Ultrafine Grained and Nanostructured Materials. 2023;56(2):213-23.
2. Radziejewska J, Marczak M, Maj P, Głowacki D, Diduszko R. Surface integrity and mechanical properties of small elements fabricated through LPBF and post-processed with heat treatment and abrasive machining. Archives of Civil and Mechanical Engineering. 2024;25(1):25.
3. Ara I, Bajwa D, Raeisi A. A review on the wear performance of additively manufactured 316L stainless steel: process, structure, and performance. Journal of Materials Science. 2025:1-35.
4. Mirzadeh H. Manufacturing of fine-grained AZ80 surface composites by friction stir processing: A review. Journal of Ultrafine Grained and Nanostructured Materials. 2025 Jun 1;58(1):33-44.
5. Sedaghat R, Mazaheri Y, Anjabin N, Ebrahimi R. Effect of heat treatment on anisotropic mechanical properties of 316L stainless steel produced via laser-based powder bed fusion. Journal of Ultrafine Grained and Nanostructured Materials. 2025;58(1):95-107.
6. Su J, Ng WL, An J, Yeong WY, Chua CK, Sing SL. Achieving sustainability by additive manufacturing: a state-of-the-art review and perspectives. Virtual and Physical Prototyping. 2024;19(1):e2438899.
7. Dekis M, Tawfik M, Egiza M, Dewidar M. Challenges and developments in wire arc additive manufacturing of steel: A review. Results in Engineering. 2025:104657.
8. Moura B, Monteiro H. Current development of the metal additive manufacturing sustainability–A systematic review. Environmental Impact Assessment Review. 2025;112:107778.
9. Gholamzadeh J, Fatemi SM, Mollaei N, Abedi A. Processing of Ultrafine/nano-grained microstructures through additive manufacturing techniques: a critical review. Journal of Ultrafine Grained and Nanostructured Materials. 2024 Dec 1;57(2):203-21.
10. Safavi MS, Azarniya A, Farshbaf Ahmadipour M, Reddy MV. New-emerging approach for fabrication of near net shape aluminum matrix composites/nanocomposites: Ultrasonic additive manufacturing. Journal of Ultrafine Grained and Nanostructured Materials. 2019;52(2):188-96.
11. Yap CY, Chua CK, Dong ZL, Liu ZH, Zhang DQ, Loh LE, Sing SL. Review of selective laser melting: Materials and applications. Applied physics reviews. 2015;2(4).
12. Talebi M, Razaghian A, Niroumand B, Saboori A. Effect of in-situ alloying with Si on the microstructure of a novel Ti-5Cu alloy manufactured by laser powder bed fusion. Journal of Ultrafine Grained and Nanostructured Materials. 2025;58(1):45-54.
13. El-Aziz AM, El-Hady MA, Khlifa W. Effect of high intensity ultrasonic treatment on the microstructure, corrosion and mechanical behaviour of AC7A aluminum alloy. Light Metals 2016. 2016:721-4.
14. Mao X, Su G, Liang X, Wang W, Qi C. The strength and ductility mechanism of gradient fine grains prepared by surface severe plastic deformation. Materials Today Communications. 2024;39:108869.
15. Keymanesh M, Ji H, Huang K, Tang M, Chen Z, Jamil MF, Feng P, Zhang J. Prediction of surface layer characteristics in ultrasonic deep cold rolling process. Advances in Engineering Software. 2025;207:103942.
16. Snopiński P. Electron microscopy study of structural defects formed in additively manufactured AlSi10Mg alloy processed by equal channel angular pressing. Symmetry. 2023 Apr 4;15(4):860.
17. Huang N, Luo Q, Bartles DL, Simpson TW, Beese AM. Effect of heat treatment on microstructure and mechanical properties of AlSi10Mg fabricated using laser powder bed fusion. Materials Science and Engineering: A. 2024 Mar 1;895:146228.
18. Baloor SS, Polishetty A, Bolar G, Govindhan AN. Heat treatment and its effect on machining induced surface roughness of cast and additive manufactured AlSi10Mg. Scientific Reports. 2025 Jul 21;15(1):1-7.
19. Ye C, Zhang C, Zhao J, Dong Y. Effects of post-processing on the surface finish, porosity, residual stresses, and fatigue performance of additive manufactured metals: a review. Journal of Materials Engineering and Performance. 2021;30(9):6407-25.
20. Aksenov DA, Nazarov AA, Raab GI, Raab AG, Fakhretdinova EI, Asfandiyarov RN, Shishkunova MA, Sementeeva YR. Effects of severe plastic deformation and ultrasonic treatment on the structure, strength, and corrosion resistance of Mg-Al-Zn alloy. Materials. 2022;15(20):7200.
21. Zhang C, Ouyang D, Pauly S, Liu L. 3D printing of bulk metallic glasses. Materials Science and Engineering: R: Reports. 2021;145:100625.
22. Newton L. Development of methods for measuring and characterising the surface topography of additively manufactured parts; PhD Thesis, University of Nottingham;2020.
23. Sefene EM. State-of-the-art of selective laser melting process: A comprehensive review. Journal of Manufacturing Systems. 2022;63:250-74.
24. Gunasekaran J, Sevvel P, Solomon IJ, Tanushkumaar P. A brief review on the manufacturing of metal components using selective laser melting. Materials Today: Proceedings. 2022;64:173-80.
25. Soni N, Renna G, Leo P. Advancements in metal processing additive technologies: selective laser melting (SLM). Metals. 2024;14(9):1081.
26. Zhang LC, Attar H, Calin M, Eckert J. Review on manufacture by selective laser melting and properties of titanium based materials for biomedical applications. Materials Technology. 2016;31(2):66-76.
27. Yang G, Xie Y, Zhao S, Qin L, Wang X, Wu B. Quality control: Internal defects formation mechanism of selective laser melting

based on laser-powder-melt pool interaction: A review. Chinese Journal of Mechanical Engineering: Additive Manufacturing Frontiers. 2022;1(3):100037.
28. Kaynak Y, Kitay O. The effect of post-processing operations on surface characteristics of 316L stainless steel produced by selective laser melting. Additive Manufacturing. 2019;26:84-93.
29. Ge J, Pillay S, Ning H. Post-process treatments for additive-manufactured metallic structures: a comprehensive review. Journal of Materials Engineering and Performance. 2023;32(16):7073-122.
30. Bajaj D, Feng A, Qu S, Chen Z, Li D, Chen DL. Deformation behavior of 3D-printed high-entropy alloys: a critical review. Advanced Engineering Materials. 2024;26(4):2300615.
31. Chowdhury S, Yadaiah N, Prakash C, Ramakrishna S, Dixit S, Gupta LR, Buddhi D. Laser powder bed fusion: a state-of-the-art review of the technology, materials, properties & defects, and numerical modelling. Journal of Materials Research and Technology. 2022;20:2109-72.
32. Yeganeh M, Shahryari Z, Talib Khanjar A, Hajizadeh Z, Shabani F. Inclusions and segregations in the selective Laser-melted alloys: a review. Coatings. 2023;13(7):1295.
33. Zhong Y, Liu L, Wikman S, Cui D, Shen Z. Intragranular cellular segregation network structure strengthening 316L stainless steel prepared by selective laser melting. Journal of Nuclear Materials. 2016;470:170-8.
34. Abramova MM, Enikeev NA, Valiev RZ, Etienne A, Radiguet B, Ivanisenko Y, Sauvage X. Grain boundary segregation induced strengthening of an ultrafine-grained austenitic stainless steel. Materials letters. 2014;136:349-52.
35. Yu X, Lin X, Liu F, Wang L, Tang Y, Li J, Zhang S, Huang W. Influence of post-heat-treatment on the microstructure and fracture toughness properties of Inconel 718 fabricated with laser directed energy deposition additive manufacturing. Materials Science and Engineering: A. 2020;798:140092.
36. Lopez-Galilea I, Ruttert B, He J, Hammerschmidt T, Drautz R, Gault B, Theisen W. Additive manufacturing of CMSX-4 Ni-base superalloy by selective laser melting: Influence of processing parameters and heat treatment. Additive Manufacturing. 2019;30:100874.
37. de Formanoir C, Michotte S, Rigo O, Germain L, Godet S. Electron beam melted Ti–6Al–4V: Microstructure, texture and mechanical behavior of the as-built and heat-treated material. Materials Science and Engineering: A. 2016;652:105-19.
38. Li W, Wu D, Hu K, Xu Y, Yang X, Zhang Y. A comparative study on the employment of heat treatment, electric pulse processing and friction stir processing to enhance mechanical properties of cold-spray-additive-manufactured copper. Surface and Coatings Technology. 2021;409:126887.
39. Beretta S, Romano S. A comparison of fatigue strength sensitivity to defects for materials manufactured by AM or traditional processes. International Journal of Fatigue. 2017;94:178-91.
40. Liu S, Shin YC. Additive manufacturing of Ti6Al4V alloy: A review. Materials & Design. 2019;164:107552.
41. Kok Y, Tan XP, Wang P, Nai ML, Loh NH, Liu E, Tor SB. Anisotropy and heterogeneity of microstructure and mechanical properties in metal additive manufacturing: A critical review. Materials & Design. 2018;139:565-86.
42. Zhang M, Liu C, Shi X, Chen X, Chen C, Zuo J, Lu J, Ma S. Residual stress, defects and grain morphology of Ti-6Al-4V alloy produced by ultrasonic impact treatment assisted selective laser melting. Applied sciences. 2016;6(11):304.
43. Ansarian I, Taghiabadi R, Amini S, Mosallanejad MH, Iuliano L, Saboori A. Improvement of surface mechanical and tribological characteristics of L-PBF processed commercially pure titanium through ultrasonic impact treatment. Acta Metallurgica Sinica (English Letters). 2024;37(6):1034-46.
44. Lesyk DA, Martinez S, Mordyuk BN, Pedash OO, Dzhemelinskyi VV, Lamikiz A. Ultrasonic surface post-processing of hot isostatic pressed and heat treated superalloy parts manufactured by laser powder bed fusion. Additive Manufacturing Letters. 2022;3:100063.
45. Lesyk D, Mordyuk B, Martinez S, Dzhemelinskyi V, Grochala D, Kotko A, Lamikiz A. Enhancing the surface integrity of a laser powder bed fusion inconel 718 alloy by tailoring the microstructure and microrelief using various finishing methods. Coatings. 2025;15(4):425.
46. Kumar H, Singh G. Parametric studies on finishing of inconel 718 flat surfaces with chemically assisted magnetic abrasive finishing process. Materials Today: Proceedings. 2021;37:3262-9.
47. Mohammadian N, Turenne S, Brailovski V. Surface finish control of additively-manufactured Inconel 625 components using combined chemical-abrasive flow polishing. Journal of Materials Processing Technology. 2018;252:728-38.
48. Trdan U, Hočevar M, Gregorčič P. Transition from superhydrophilic to superhydrophobic state of laser textured stainless steel surface and its effect on corrosion resistance. Corrosion science. 2017;123:21-6.
49. Obeidi MA, Conway A, Mussatto A, Dogu MN, Sreenilayam SP, Ayub H, Ahad IU, Brabazon D. Effects of powder compression and laser re-melting on the microstructure and mechanical properties of additively manufactured parts in laser-powder bed fusion. Results in Materials. 2022;13:100264.
50. Metelkova J, Vanmunster L, Haitjema H, Ordnung D, Kruth JP, Van Hooreweder B. Hybrid dual laser processing for improved quality of inclined up-facing surfaces in laser powder bed fusion of metals. Journal of Materials Processing Technology. 2021;298:117263.
51. Edalati K, Ahmed AQ, Akrami S, Ameyama K, Aptukov V, Asfandiyarov RN, Ashida M, Astanin V, Bachmaier A, Beloshenko V, Bobruk EV. Severe plastic deformation for producing superfunctional ultrafine-grained and heterostructured materials: an interdisciplinary review. Journal of Alloys and Compounds. 2024;1002:174667.
52. Fatemi M, Zarei-Hanzaki A. Review on ultrafined/nanostructured magnesium alloys produced through severe plastic deformation: microstructures. Journal of Ultrafine Grained and Nanostructured Materials. 2015;48(2):69-83.
53. Edalati K, Bachmaier A, Beloshenko VA, Beygelzimer Y, Blank VD, Botta WJ, Bryła K, Čížek J, Divinski S, Enikeev NA, Estrin Y. Nanomaterials by severe plastic deformation: review of historical developments and recent advances. Materials Research Letters. 2022;10(4):163-256.
54. Edalati K, Horita Z. Recent research trends in severe plastic deformation of metallic and non-metallic materials. Materials Transactions. 2025;66(4):450-61.
55. Acharya S, Suwas S, Chatterjee K. Review of recent developments in surface nanocrystallization of metallic biomaterials. Nanoscale. 2021;13(4):2286-301.
56. Keymanesh M, Ji H, Tang M, Zhang X, Huang K, Wang J, Feng P, Zhang J. Ultrasonic surface treatment techniques based on cold working: a review. The International Journal of Advanced Manufacturing Technology. 2024;134(11):4949-79.
57. Nemati R, Taghiabadi R, Saghafi Yazdi M, Amini S. Tribology characteristics of ultrasonic impact treated Co-Based L-605 superalloy. Iranian Journal of Materials Forming. 2025;12(1):37-50.
58. Omidi Hashjin A, Vahdati M, Abedini R. Investigating the effect of ultrasonic shot peening parameters on metallurgical, mechanical, and corrosion properties of industrial parts: a literature review. Iranian Journal of Materials Forming. 2024;11(2):75-95.
59. Singh V, Pandey V, Kumar S, Srinivas NS, Chattopadhyay K. Effect of ultrasonic shot peening on surface microstructure and fatigue behavior of structural alloys. Transactions of the Indian Institute of Metals. 2016;69(2):295-301.
60. Kalantari K, Saleh B, Webster TJ. Biological applications of severely plastically deformed nano-grained medical devices: a review. Nanomaterials. 2021;11(3):748.
61. Rakita M, Wang M, Han Q, Liu Y, Yin F. Ultrasonic shot peening. International Journal of Computational Materials Science and Surface Engineering. 2013;5(3):189-209.
62. Santos V, Uddin M, Hall C. Mechanical surface treatments

for controlling surface integrity and corrosion resistance of Mg alloy implants: a review. Journal of Functional Biomaterials. 2023;14(5):242.
63. Yin FE, Hu S, Hua LI, Wang X, Suslov S, Han Q. Surface nanocrystallization and numerical modeling of low carbon steel by means of ultrasonic shot peening. Metallurgical and Materials Transactions A. 2015;46(3):1253-61.
64. Li K, He Y, Fang C, Ma H, Kim J, Lee HS, Song JI, Yang CW, Lee JH, Shin K. Surface nanocrystallization of pure Cu induced by ultrasonic shot peening. Journal of Nanoscience and Nanotechnology. 2014;14(12):9637-43.
65. Wu XL, Tao NR, Hong YS, Xu B, Lu J, Lu K. Microstructure and evolution of mechanically-induced ultrafine grain in surface layer of Al-alloy subjected to USSP. Acta materialia. 2002;50(8):2075-84.
66. Hou LF, Wei YH, Liu BS, XU BS. Microstructure evolution of AZ91D induced by high energy shot peening. Transactions of Nonferrous Metals Society of China. 2008;18(5):1053-7.
67. Liu G, Lu J, Lu K. Surface nanocrystallization of 316L stainless steel induced by ultrasonic shot peening. Materials Science and Engineering: A. 2000;286(1):91-5.
68. Austernaud Y, Novelli M, Bocher P, Grosdidier T. Effect of shot peening temperature on the microstructure induced by surface severe plastic deformation on an austenitic stainless steel. Journal of Materials Processing Technology. 2025;339:118823.
69. Pour-Ali S, Kiani-Rashid AR, Babakhani A, Virtanen S, Allieta M. Correlation between the surface coverage of severe shot peening and surface microstructural evolutions in AISI 321: A TEM, FE-SEM and GI-XRD study. Surface and Coatings Technology. 2018;334:461-70.
70. Fu T, Zhan Z, Zhang L, Yang Y, Liu Z, Liu J, Li L, Yu X. Effect of surface mechanical attrition treatment on corrosion resistance of commercial pure titanium. Surface and Coatings Technology. 2015;280:129-35.
71. Maleki E, Unal O, Guagliano M, Bagherifard S. The effects of shot peening, laser shock peening and ultrasonic nanocrystal surface modification on the fatigue strength of Inconel 718. Materials Science and Engineering: A. 2021;810:141029.
72. Zhuang W, Liu Q, Djugum R, Sharp PK, Paradowska A. Deep surface rolling for fatigue life enhancement of laser clad aircraft aluminium alloy. Applied Surface Science. 2014;320:558-62.
73. Malaki M, Ding H. A review of ultrasonic peening treatment. Materials & Design. 2015;87:1072-86.
74. John M, Kalvala PR, Misra M, Menezes PL. Peening techniques for surface modification: Processes, properties, and applications. Materials. 2021;14(14):3841.
75. Abdullah A, Malaki M, Eskandari A. Strength enhancement of the welded structures by ultrasonic peening. Materials & Design. 2012;38:7-18.
76. Yuan Y, Li R, Bi X, Yan M, Cheng J, Gu J. Review on numerical simulation of ultrasonic impact treatment (UIT): Present situation and prospect. Journal of Materials Research and Technology. 2024;30:1319-40.
77. Zeng L, Xu G, Wang C, Liang T. Microstructure and corrosion behavior of ultrasonic surface treated 7B85 Al alloy. JOM. 2023;75(1):86-96.
78. Nemati R, Taghiabadi R, Yazdi MS, Amini S. Ultrasonic impact treatment of CoCrWNi superalloys for surface properties improvement. Materials Testing. 2025;67(2):372-85.
79. Wu B, Zhang L, Zhang J, Murakami RI, Pyoun YS. An investigation of ultrasonic nanocrystal surface modification machining process by numerical simulation. Advances in Engineering Software. 2015;83:59-69.
80. Kim MS, Park SH, Pyun YS, Shim DS. Optimization of ultrasonic nanocrystal surface modification for surface quality improvement of directed energy deposited stainless steel 316L. Journal of Materials Research and Technology. 2020;9(6):15102-22.
81. Polonyankina DA, Fedorova AA, Gomonyuka TM. Phase composition of stainless steel subjected to ultrasonic nanocrystal surface modification with different processing density. Journal of Advanced Materials and Technologies. 2024;9(4):257-66.
82. Li Y, Lu Z, Li T, Li D, Lu J, Liaw PK, Zou Y. Effects of surface severe plastic deformation on the mechanical behavior of 304 stainless steel. Metals. 2020;10(6):831.
83. Zhao W, Liu D, Liu J, Zhang X, Zhang H, Zhang R, Dong Y, Ye C. The effects of laser-assisted ultrasonic nanocrystal surface modification on the microstructure and mechanical properties of 300M steel. advanced engineering materials. 2021;23(3):2001203.
84. Kishore A, John M, Ralls AM, Jose SA, Kuruveri UB, Menezes PL. Ultrasonic nanocrystal surface modification: processes, characterization, properties, and applications. Nanomaterials. 2022;12(9):1415.
85. Hong JH, Park H, Kim J, Seok MY, Choi H, Kwon YN, Lee DJ. Effect of the residual stress induced by surface severe plastic deformation on the tensile behavior of an aluminum alloy. Journal of Materials Research and Technology. 2023;24:7076-90.
86. Ansarian I, Taghiabadi R, Amini S, Saboori A. The effect of surface severe plastic deformation on microstructure and mechanical properties of pure titanium produced by selective laser melting. Founding Research Journal. 2023;7(1):15-24.
87. Ojo SA, Manigandan K, Morscher GN, Gyekenyesi AL. Enhancement of the microstructure and fatigue crack growth performance of additive manufactured titanium alloy parts by laser-assisted ultrasonic vibration processing. Journal of Materials Engineering and Performance. 2024;33(19):10345-59.
88. Chae JM, Lee KO, Amanov A. Gradient nanostructured tantalum by thermal-mechanical ultrasonic impact energy. Materials. 2018;11(3):452.
89. Nemati R, Taghiabadi R, Saghafi Yazdi M, Amini S. Corrosion behavior of ultrasonic impact treated Haynes 25 superalloy. Journal of Ultrafine Grained and Nanostructured Materials. 2025;58(1):67-77.
90. Nemati R, Taghiabadi R, Saghafi Yazdi M, Amini S. Tribology characteristics of ultrasonic impact treated Co-Based L-605 superalloy. Iranian Journal of Materials Forming. 2025;12(1):37-50.
91. Suh CM, Song GH, Park HD, Pyoun YS. A study of the mechanical characteristics of ultrasonic cold forged SKD61. International Journal of Modern Physics B. 200620(25n27):4541-6.
92. Suh CM, Song GH, Pyoun YS. A quality control method by ultrasonic vibration energy and diagnosis system at trimming process. Journal of Mechanical Science and Technology. 2007;21(3):397-402.
93. Chen L, Gu Y, Liu L, Liu S, Hou B, Liu Q, Ding H. Effect of ultrasonic cold forging technology as the pretreatment on the corrosion resistance of MAO Ca/P coating on AZ31B Mg alloy. Journal of Alloys and Compounds. 2015;635:278-88.
94. Suh CM, Song GH, Suh MS, Pyoun YS. Fatigue and mechanical characteristics of nano-structured tool steel by ultrasonic cold forging technology. Materials Science and Engineering: A. 2007;443(1-2):101-6.
95. Suh CM, Song GH, Suh MS, Pyoun YS, Kim MH. Mechanical characteristics of nano-structured tool steel by ultrasonic cold forging technology. The Korea Committee for Ocean Resources and Engineering Conference; Korean Society of Ocean Engineers; 2006: 35-40, Busan, Korea.
96. Mordyuk BN, Prokopenko GI. Fatigue life improvement of α-titanium by novel ultrasonically assisted technique. Materials Science and Engineering: A. 2006;437(2):396-405.
97. Wang H, Jerez-Mesa R, Velázquez-Corral E, Wang X. Ultrasonic rolling strengthening theory and mechanism analysis of high-strength 42CrMo steel. Archives of Civil and Mechanical Engineering. 2025;25(3):1-30.
98. Yang Y, Huang T, Ye C, Ding H. Recent progress in ultrasonic surface rolling: a comprehensive overview. Advanced Engineering Materials. 2024;26(22):2401100.
99. Zhang Y, Zhan M, Fan X. Deepening the cognition of ultrasonic vibration's role on plastic deformation of 2219 aluminum alloy tube during ultrasonic surface rolling process. Manufacturing Review. 2024;11:23.
100. Ma X, Zhang W, Xu S, Sun K, Hu X, Ren G, Li J, Zhao X,

Gao F. Effect of ultrasonic surface rolling process on surface properties and microstructure of 6061 aluminum alloy. Materials Research. 2023;26:e20230322.
101. Zhang Y, Wu L, Shi D, Wang Z, Jin H, Liu L, Qu S, Ji V. Surface integrity and tribological behavior of 17Cr2Ni2MoVNb steel under combined carburizing treatment and ultrasonic rolling. Surface and Coatings Technology. 2023;461:129371.
102. Yang Y, Huang T, Ye C, Ding H. Recent progress in ultrasonic surface rolling: a comprehensive overview. Advanced Engineering Materials. 2024;26(22):2401100.
103. Cheng Y, Wang Y, Wang Z, Huang P, Zhang P, Guo Q. Ultrasonic surface rolling strengthening and its parameter optimization on bearing raceway. Materials & Design. 2023;232:112156.
104. Wang B, Yin Y, Gao Z, Hou Z, Jiang W. Influence of the ultrasonic surface rolling process on stress corrosion cracking susceptibility of high strength pipeline steel in neutral pH environment. RSC Advances. 2017;7(59):36876-85.
105. Kumaravelu P, Arulvel S, Kandasamy J. Surface coatings and surface modification Techniques for Additive Manufacturing. Innovations in Additive Manufacturing. 2022:221-38.
106. John M, Ralls AM, Dooley SC, Thazhathidathil AK, Perka AK, Kuruveri UB, Menezes PL. Ultrasonic surface rolling process: Properties, characterization, and applications. Applied Sciences. 2021;11(22):10986.
107. Wang J, Qu S, Lai F, Deng Y, Li X. Effect of ultrasonic surface rolling on microstructural evolution and fretting wear resistance of 20CrMoH steel under different quenching temperatures. Materials Chemistry and Physics. 2022;288:126362.
108. Zhang Y, Huang L, Lu F, Qu S, Ji V, Hu X, Liu H. Effects of ultrasonic surface rolling on fretting wear behaviors of a novel 25CrNi2MoV steel. Materials Letters. 2021;284:128955.
109. Li L, Zhang W, Jiang GQ, Meng XK, Zhang HM, Li PF, Huang S, Zhou JZ. Effects of ultrasonic surface rolling process on the microstructure and wear resistance of 2195 Al-Li alloy processed by laser powder bed fusion. Materials Letters. 2025;379:137732.
110. Li L, Huang L, Wu J, Dai L, Meng X, Zhang H, Li P, Huang S, Zhou J. Effect of ultrasonic surface rolling on the microstructure and mechanical properties of 2195 Al-Li alloy fabricated by laser powder bed fusion in various build directions. Journal of Alloys and Compounds. 2024;1008:176869.
111. Huang L, Gou Y, Li L, Zhou J, Meng X, Huang S. Study on gradient structure and surface strengthening mechanism of LPBF 2099 Al-Li alloy induced by ultrasonic surface rolling. Journal of Alloys and Compounds. 2025;1022:179778.
112. Tan L, Tang W, Wang M, Zhang Y, Yao C. Studies on surface integrity and fatigue performance of Ti-17 alloy induced by ultrasonic surface rolling process. Surface and Coatings Technology. 2025:132336.
113. Li G, Qu S, Guan S, Wang F. Study on the tensile and fatigue properties of the heat-treated HIP Ti-6Al-4V alloy after ultrasonic surface rolling treatment. Surface and Coatings Technology. 2019;379:124971.
114. Ren Z, Lai F, Qu S, Zhang Y, Li X, Yang C. Effect of ultrasonic surface rolling on surface layer properties and fretting wear properties of titanium alloy Ti5Al4Mo6V2Nb1Fe. Surface and Coatings Technology. 2020;389:125612.
115. Ye H, Sun X, Liu Y, Rao XX, Gu Q. Effect of ultrasonic surface rolling process on mechanical properties and corrosion resistance of AZ31B Mg alloy. Surface and Coatings Technology. 2019;372:288-98.
116. Li X, Wang X, Liu L, Huang Z, Bai J, Zhang X, Liang T. Effect of ultrasonic surface rolling process on microstructure and surface properties of Cu-8 wt.% Al alloy. Materials Science and Technology. 2024:02670836251349870.
117. Li X, Wang X, Chen B, Gao M, Jiang C, Yuan H, Zhang X, Liang T. Effect of ultrasonic surface rolling process on the surface properties of CuCr alloy. Vacuum. 2023;209:111819.
118. Xie J, Zhang S, Sun Y, Hao Y, An B, Li Q, Wang CA. Microstructure and mechanical properties of high entropy CrMnFeCoNi alloy processed by electopulsing-assisted ultrasonic surface rolling. Materials Science and Engineering: A. 2020;795:140004.
119. Li W, Shi X, Liang Y, Zhang Z, Cui J. Effects of ultrasonic surface rolling processing on the surface microstructure and properties of a tungsten heavy alloy. Materials Research Express. 2019;6(12):1265a5.
120. Chen H, Sun S, Tian F, Dou M, Liu L, Li L. Deformation mechanism of Ni-based single crystal superalloy under ultrasonic surface rolling and subsequent thermal exposure. Surface and Coatings Technology. 2024;494:131369.
121. Sun J, Zhang Y, Sun Z, Yu T, Wang G. Microstructure and tribological property of laser cladding Stellite 6 alloy by laser remelting and ultrasonic surface rolling. Surface and Coatings Technology. 2025;495:131560.
122. Bozdana AT, Gindy NN, Li H. Deep cold rolling with ultrasonic vibrations—a new mechanical surface enhancement technique. International Journal of Machine tools and manufacture. 2005;45(6):713-8.
123. Bozdana AT, Gindy NN. Comparative experimental study on effects of conventional and ultrasonic deep cold rolling processes on Ti–6Al–4V. Materials Science and Technology. 2008;24(11):1378-84.
124. Keymanesh M, Ji H, Huang K, Tang M, Chen Z, Jamil MF, Feng P, Zhang J. Prediction of surface layer characteristics in ultrasonic deep cold rolling process. Advances in Engineering Software. 2025;207:103942.
125. Alam Z, Iqbal F, Khan DA, editors. Post-processing techniques for additive manufacturing. CRC Press; 2023.
126. Zhang Q, Duan B, Zhang Z, Wang J, Si C. Effect of ultrasonic shot peening on microstructure evolution and corrosion resistance of selective laser melted Ti–6Al–4V alloy. Journal of Materials Research and Technology. 2021;11:1090-9.
127. Alharbi N. Shot peening of selective laser-melted SS316L with ultrasonic frequency. The International Journal of Advanced Manufacturing Technology. 2022;119(3):2285-99.
128. Alharbi N. Corrosion resistance of 3D printed SS316L post-processed by ultrasonic shot peening at optimum energy level. Proceedings of the Institution of Mechanical Engineers, Part B: Journal of Engineering Manufacture. 2023;237(5):745-57.
129. Xu ZB, Zeng XY, Xu X, Wu H. Application study of improving wear resistance of selective laser melting 316L stainless steel by ultrasonic shot peening technology. Journal of Materials Engineering and Performance. 2025:1-4.
130. Yu T, Chen L, Zhang X, Zhu L, Li Y, Ren X. Effect of ultrasonic shot peening on microstructure and mechanical properties of GH3230 superalloy during selective laser melt solution heat treatment. Materials Today Communications. 2024;39:108850.
131. Srikanth M, Charan BS, Venu DM, Venkatesan K, Sreedhar G, Chattopadhyay K, Pattanayak DK. Enhancement of high temperature oxidation and hot corrosion resistance behaviors of selective laser melted Ti6Al4V by ultrasonic shot peening. Materials Chemistry and Physics. 2025;332:130170.
132. Yan X, Yin S, Chen C, Jenkins R, Lupoi R, Bolot R, Ma W, Kuang M, Liao H, Lu J, Liu M. Fatigue strength improvement of selective laser melted Ti6Al4V using ultrasonic surface mechanical attrition. Materials Research Letters. 2019;7(8):327-33.
133. Portella Q, Chemkhi M, Retraint D. Influence of surface mechanical attrition treatment (SMAT) post-treatment on microstructural, mechanical and tensile behaviour of additive manufactured AISI 316L. Materials Characterization. 2020;167:110463.
134. Kan WH, Portella Q, Chemkhi M, Proust G, Garbrecht M, Cairney JM, Retraint D. Enhancing mechanical properties of laser powder bed fused 316L stainless steel through heat and surface mechanical attrition treatments. Materials Science and Engineering: A. 2024;910:146862.
135. Ghosh S, Bibhanshu N, Suwas S, Chatterjee K. Surface mechanical attrition treatment of additively manufactured 316L stainless steel yields gradient nanostructure with superior strength and ductility. Materials Science and Engineering: A.

2021;820:141540.
136. Lesyk DA, Martinez S, Mordyuk BN, Dzhemelinskyi VV, Lamikiz A, Prokopenko GI. Post-processing of the Inconel 718 alloy parts fabricated by selective laser melting: Effects of mechanical surface treatments on surface topography, porosity, hardness and residual stress. Surface and Coatings Technology. 2020;381:125136.
137. Zhang Q, Xu S, Wang J, Zhang X, Wang J, Si C. Microstructure change and corrosion resistance of selective laser melted Ti-6Al-4V alloy subjected to pneumatic shot peening and ultrasonic shot peening. Surface Topography: Metrology and Properties. 2022;10(1):015010.
138. Liu W, Shen S, Meng J, Xiao J, Li H, Du H, Yin Q, Tan C. Mechanical field assisted additive manufacturing of ultrahigh strength aluminum alloy. International Journal of Extreme Manufacturing. 2025;7(4):045008.
139. Zhang H, Zhao J, Liu J, Qin H, Ren Z, Doll GL, Dong Y, Ye C. The effects of electrically-assisted ultrasonic nanocrystal surface modification on 3D-printed Ti-6Al-4V alloy. Additive Manufacturing. 2018;22:60-8.
140. Kim RE, Jeong SG, Ha H, Lee DW, Amanov A, Kim HS. Controlling defects of laser-powder bed fusion processed 316L stainless steel via ultrasonic nanocrystalline surface modification. Materials Science and Engineering: A. 2023;887:145726.
141. Amanov A, Pyun YS. Local heat treatment with and without ultrasonic nanocrystal surface modification of Ti-6Al-4V alloy: Mechanical and tribological properties. Surface and Coatings Technology. 2017;326:343-54.
142. Cho SY, Kim MS, Pyun YS, Shim DS. Strategy for surface post-processing of AISI 316L additively manufactured by powder bed fusion using ultrasonic nanocrystal surface modification. Metals. 2021;11(5):843.
143. Gilmore RW. An Evaluation of ultrasonic shot peening and abrasive flow machining as surface finishing processes for selective laser melted 316L. M.Sc. thesis, California Polytechnic State University;2018.
144. Karimbaev RM, Cho IS, Pyun YS, Amanov A. Effect of ultrasonic nanocrystal surface modification treatment at room and high temperatures on the high-frequency fatigue behavior of Inconel 718 fabricated by laser metal deposition. Metals. 2022;12(3):515.
145. Ma C, Andani MT, Qin H, Moghaddam NS, Ibrahim H, Jahadakbar A, Amerinatanzi A, Ren Z, Zhang H, Doll GL, Dong Y. Improving surface finish and wear resistance of additive manufactured nickel-titanium by ultrasonic nano-crystal surface modification. Journal of Materials Processing Technology. 2017;249:433-40.
146. Kim MS, Oh WJ, Baek GY, Jo YK, Lee KY, Park SH, Shim DS. Ultrasonic nanocrystal surface modification of high-speed tool steel (AISI M4) layered via direct energy deposition. Journal of Materials Processing Technology. 2020;277:116420.
147. Zhang H, Chiang R, Qin H, Ren Z, Hou X, Lin D, Doll GL, Vasudevan VK, Dong Y, Ye C. The effects of ultrasonic nanocrystal surface modification on the fatigue performance of 3D-printed Ti64. International Journal of Fatigue. 2017;103:136-46.
148. Ma C, Dong Y, Ye C. Improving surface finish of 3D-printed metals by ultrasonic nanocrystal surface modification. Procedia Cirp. 2016;45:319-22.
149. Karimbaev RM, Pyun YS, Amanov A. Fatigue life extension of additively manufactured Nickel-base 718 alloy by nanostructured surface. Materials Science and Engineering: A. 2022;831:142041.
150. Amanov A, Yeo IK, Jeong S. Individual and dual applications of laser shock peening and ultrasonic nanocrystal surface modification technologies to Ti-6Al-4V alloy manufactured by selective laser melting. Available at SSRN 4512662.
151. Zhang H, Zhao J, Liu J, Qin H, Ren Z, Doll GL, Dong Y, Ye C. The effects of electrically-assisted ultrasonic nanocrystal surface modification on 3D-printed Ti-6Al-4V alloy. Additive Manufacturing. 2018;22:60-8.
152. Amanov A. Effect of post-additive manufacturing surface modification temperature on the tribological and tribocorrosion properties of Co-Cr-Mo alloy for biomedical applications. Surface and Coatings Technology. 2021;421:127378.
153. Ansarian I, Taghiabadi R, Amini S, Saboori A. Enhancing the corrosion behavior of laser powder bed fusion processed CP-Ti via ultrasonic peening. Materials Letters. 2024;354:135410.
154. Liu W, Li H, Yin Q, Zhou X. Promoting densification and strengthening effect of ultrasonic impact treatment on Haynes 230 alloy manufactured by laser powder bed fusion. Journal of Materials Science & Technology. 2025;216:226-40.
155. Xing X, Duan X, Jiang T, Wang J, Jiang F. Ultrasonic peening treatment used to improve stress corrosion resistance of AlSi10Mg components fabricated using selective laser melting. Metals. 2019;9(1):103.
156. Lesyk D, Mordyuk B, Grinkevych K, Pedash O, Lamikiz A. Effects of multi-pin ultrasonic peening, shot peening and hot isostatic pressing on wear resistance of Inconel 718 alloy manufactured by laser powder bed fusion. design, simulation, manufacturing: The Innovation Exchange. 2025:57-67. Springer Nature Switzerland.
157. Yang X, Xu S, Liu R. Effect of ultrasonic surface rolling process on surface integrity and corrosion resistance of laser powder bed fusion 316L stainless steel under different static load forces. Journal of Materials Engineering and Performance. 2025:1-2.
158. Chen X, Lu T, Yao N, Chen H, Sun B, Xie Y, Chen Y, Wan B, Zhang XC, Tu ST. Enhanced fatigue resistance and fatigue-induced substructures in an additively manufactured CoCrNi medium-entropy alloy treated by ultrasonic surface rolling process. International Journal of Plasticity. 2023;169:103721.
159. Xu Q, Jiang D, Zhou J, Qiu Z, Yang X. Enhanced corrosion resistance of laser additive manufactured 316L stainless steel by ultrasonic surface rolling process. Surface and Coatings Technology. 2023;454:129187.
160. Wang Z, Liu Z, Gao C, Wong K, Ye S, Xiao Z. Modified wear behavior of selective laser melted Ti6Al4V alloy by direct current assisted ultrasonic surface rolling process. Surface and Coatings Technology. 2020;381:125122.
161. Liu G, Su YG, Pi XY, Wen DX, Liu DF, Lin YC. Enhanced electrochemical corrosion resistance of 316L stainless steel manufactured by ultrasonic rolling assisted laser directed energy deposition. China Foundry. 2025;22(2):182-94.
162. Liu Z, Gao C, Liu X, Liu R, Xiao Z. Improved surface integrity of Ti6Al4V fabricated by selective electron beam melting using ultrasonic surface rolling processing. Journal of Materials Processing Technology. 2021;297:117264.
163. Qian B, Dai P, Zhao M, Cui Q, Liu G, Wei Q, Li R, Liang SY. Mechanism of microstructure and mechanical properties improvement through ultrasonic rolling pressing layer-by-layer and adaptive ultrasonic rolling method research in AlSi10Mg laser powder bed fused. Journal of Materials Research and Technology. 2025.
164. Salmi M, Huuki J, Ituarte IF. The ultrasonic burnishing of cobalt-chrome and stainless steel surface made by additive manufacturing. Progress in Additive Manufacturing. 2017;2(1):31-41.
165. Wang J, Geng Y, Li Z, Yan Y, Luo X, Fan P. Study on the vertical ultrasonic vibration-assisted nanomachining process on single-crystal silicon. Journal of Manufacturing Science and Engineering. 2022;144(4):041013.
166. Teramachi A, Yan J. Improving the surface integrity of additive-manufactured metal parts by ultrasonic vibration-assisted burnishing. Journal of micro-and nano-manufacturing. 2019;7(2):024501.
167. Ituarte IF, Salmi M, Papula S, Huuki J, Hemming B, Coatanea E, Nurmi S, Virkkunen I. Surface modification of additively manufactured 18% nickel maraging steel by ultrasonic vibration-assisted ball burnishing. Journal of Manufacturing Science and Engineering. 2020;142(7).
168. Velázquez E, Travieso-Disotuar A, Jerez-Mesa R, Vilaseca M, Keller C, Dessein G. Roughness and microstructure characterization of AISI 316L laser-powder bed fusion specimens

after applying a vibration-assisted ball burnishing process. Journal of Materials and Manufacturing. 2024;3(2):32-40.
169. Wang J, Zhu J, Liew PJ. Material removal in ultrasonic abrasive polishing of additive manufactured components. Applied Sciences. 2019;9(24):5359.
170. Tan KL, Yeo SH. Surface finishing on IN625 additively manufactured surfaces by combined ultrasonic cavitation and abrasion. Additive Manufacturing. 2020;31:100938.
171. Wang J, Geng Y, Li Z, Yan Y, Luo X, Fan P. Study on the vertical ultrasonic vibration-assisted nanomachining process on single-crystal silicon. Journal of Manufacturing Science and Engineering. 2022;144(4):041013.